creative commons
COMMONS DEED

저작자표시-비영리-변경금지 2.0 대한민국

이용자는 아래의 조건을 따르는 경우에 한하여 자유롭게

- 이 저작물을 복제, 배포, 전송, 전시, 공연 및 방송할 수 있습니다.

다음과 같은 조건을 따라야 합니다:

저작자표시. 귀하는 원저작자를 표시하여야 합니다.

비영리. 귀하는 이 저작물을 영리 목적으로 이용할 수 없습니다.

변경금지. 귀하는 이 저작물을 개작, 변형 또는 가공할 수 없습니다.

- 귀하는, 이 저작물의 재이용이나 배포의 경우, 이 저작물에 적용된 이용허락조건을 명확하게 나타내어야 합니다.
- 저작권자로부터 별도의 허가를 받으면 이러한 조건들은 적용되지 않습니다.

저작권법에 따른 이용자의 권리는 위의 내용에 의하여 영향을 받지 않습니다.

이것은 이용허락규약(Legal Code)을 이해하기 쉽게 요약한 것입니다.

Disclaimer

dCollection

Seoul National University
Lab. of Physics and Chemistry of Earth Materials

Master of Science Thesis

이학석사 학위논문

Effect of Ti on structure of Ti-bearing sodium aluminosilicate melts using multi-nuclear NMR spectroscopy: implication for lunar mantle dynamics

다핵종 자기 공명 분광법을 이용한 Ti 이 미치는 알루미늄 규산염 용융체 원자구조 연구: 달 맨틀 역학에 대한 고찰

August 2022

Department of Earth and Environmental Sciences
College of Natural Sciences
Seoul National University

El Ghazaoui, Elias

Effect of Ti on structure of Ti-bearing sodium aluminosilicate melts using multi-nuclear NMR spectroscopy: implication for lunar mantle dynamics

다핵종 자기 공명 분광법을 이용한 Ti 이 미치는 알루미늄 규산염 용융체 원자구조 연구: 달 맨틀 역학에 대한 고찰

지도 교수 이 성 근

이 논문을 이학석사 학위논문으로 제출함

2022 년 6 월

서울대학교 대학원

자연과학대학 지구환경과학부

El Ghazaoui, Elias

El Ghazaoui, Elias 의

이학석사 학위논문을 인준함

2022 년 6 월

위 원 장 이 준 기 (인)

부위원장 이 성 근 (인)

위 원 김 영 희 (인)

Abstract

Effect of Ti on structure of Ti-bearing sodium aluminosilicate melts using multi-nuclear NMR spectroscopy: implication for lunar mantle dynamics

El Ghazaoui, Elias

School of Earth and Environmental Sciences

Seoul National University

The evolution of the lunar mantle melts since the moon-forming giant impact event remains poorly understood. The mantle melts contain substantially more Ti compared to melts found on Earth. Therefore, evolution of the Moon might be affected by its Ti-rich mantle, as melt properties like viscosity and density are most likely influenced by these compositional changes. By incorporating Ti in simple Na trisilicate glasses and sodium aluminosilicate glasses, structural changes in this glass can be observed. This allows us to provide more information about the possible influence of Ti on the physical properties of the lunar melts. To obtain structural information from the Ti-bearing Na trisilicate glass, ^{29}Si- ^{17}O- and ^{27}Al high resolution Nuclear Magnetic Resonance(NMR) spectroscopy were used. The ^{29}Si NMR technique reveals detailed structures around the Si environment, particularly Q^n species information where n is the number of Bridging Oxygen(BO) of a single Si tetrahedron. The ^{17}O NMR technique provides detailed information about the O-bonds within the glass samples.

In general terms, Ti(network former) replaces the amount of Na(network modifier) in the glass while the amount of Si remains unchanged. For the endmember Na trisilicate(x=0), at -90 ppm and -104 ppm, two peaks appear on the ^{29}Si NMR spectra that represent Q^3 and Q^4 species respectively where

the Q^3 peak at -90 ppm is more dominant. This Q^3 peak has a Q fraction of around 0.6 while the peak representing Q^4 makes up the remaining fraction. Overall, the Q^4 peak increases at the expense of the Q^3 peak with increasing the Ti content. When 18.75 mol% Ti is incorporated in the glass, the Q species fractionation has completely changed where the Q^4 species clearly became the dominant fraction. This suggests that the number of Si surrounded by only BO would increase resulting in an increase of the network polymerization of the melt. From the ^{17}O data a similar observation can be made. The Na-O-Si bonds are gradually replaced by Si-O-Si and Ti-O-Si bonds with increasing Ti content. Also, some fraction of Ti-O-Ti forms. For the aluminosilicate glasses, no Ti-O-Al bond was observed indicating a clear titanium and aluminium avoidance.

The obtained structural knowledge regarding the incorporation of Ti on the network polymerization of the silicate glasses, allows us to make a direct link between the Ti content and the viscosity of the melt. Less upper mantle mixing could affect the previously believed timespan of magma ocean cooling to be much longer as heat is meanly being transferred with conduction. Because of the Lunar mantle overturn model driven by the higher density of the IBC layer, Ti coordination is believed to change from $^{[4]}Ti$ to $^{[6]}Ti$. The Ti becomes a network modifier, lowering the viscosity of the melt with increased mantle mixing in the lower mantle. The simple melt used in this study lays a solid foundation for further research regarding lunar melts with a more realistic melt composition or environmental conditions and could therefore help to constrain the possibilities of lunar mantle dynamics and lunar magma ocean evolution.

Keywords: Titanium sodium silicate glass, titanium sodium aluminosilicate glass, solid-state NMR spectroscopy, atomic structure, lunar glass, lunar magma ocean evolution, lunar mantle dynamics

Student number: 2022-25430

Contents

Abstract **2**

1. Introduction **10**

1.1. Understanding the lunar interior 10

1.2. Effects of Ti on the structure of glasses 19

2. Experimental methods **24**

2.1. Sample composition 24

2.2. Heating and quenching 26

2.3. XRD analyses 28

2.4. NMR Spectroscopy 30

3. Results **31**

3.1. Ti-bearing sodium trisilicate glasses 31

3.2. Ti-bearing sodium aluminosilicate glasses 38

4. Discussion **47**

4.1. Q species fitting 47

4.2. Glass network structure 49

4.3. Geological implications 52

5. Conclusion **55**

5.1. The effect of Ti on sodium tri- and aluminosilicate glasses. 55

5.2. Lunar mantle dynamics implications 55

6. Appendix section **57**

References **63**

List of figures

Figure 1. Schematic illustration that represents the lunar magma ocean evolution (E. El Ghazaoui, 2021)

Figure 2. X-ray diffraction spectra for rutile and NTS_3 glass containing 18.75 mol% Ti. No clear peak is visible in the glass sample meaning that there is no crystalline material present. Despite having a high Ti concentration, the synthesis was successful.

Figure 3. Showing in this figure are the ^{29}Si MAS NMR spectra which shows the effect of substituting Ti for Na in NS_3 glass for the Ti-bearing sodium trisilicate glasses in set 1. A clear peak intensity increase is visible for the Q^4 peak with a frequency of -104 ppm at the cost of the Q^3 peak at -90 ppm. This indicates a change in Q species with increasing Ti content in the samples. Both peaks clearly show a shift towards lower frequencies.

Figure 4. The 2D ^{17}O 3QMAS NMR spectra of titanium-bearing sodium trisilicate glasses at 9.4 T with varying XTi [$(Na_{1-x}Ti_x)$ $3{\cdot}SiO_2$] as given in the figure. The spectra showing an increasing fraction of BO(Si-O-Si and Ti-O-Si) with increasing Ti content. At Ti=0.1 a new broad peak appears around 110

ppm which later increases in intensity and shifts towards higher frequencies. The already existing peaks are both shifting the opposite direction.

Figure 5. ^{17}O 3QMAS NMR spectra for Ti-bearing sodium trisilicate glass in two dimensions; the MAS dimension and Isotropic dimension. With increasing Ti, similarly to MAS spectrum alone, it can be observed that a new peak appears representing Ti-O-Si bonds. The big difference from the 1D and 2D spectra is that the Na-O-Si bonds and Si-O-Si bonds appear as separate peaks that are distinguishable in the isotropic dimension. The 2D ^{17}O 3QMAS NMR spectra of titanium-bearing sodium trisilicate glasses at 9.4 T with varying XTi [$(Na_{1-x}Ti_x)$ $3{\cdot}SiO_2$] as given in the figure. The contour lines range from 3% to 13% and 13% to 83% relative intensity with increments of 2% and 5% respectively. For x = 0.1, a contour line of 2% is used instead of 83% to better visualize the presence of a small Ti-O-Ti peak.

Figure 6. The ^{29}Si MAS NMR spectra show the effect of substituting Ti for Al in sodium aluminosilicate glass of set 2. It starts with the Al-rich endmember also known as nepheline. No clear peak intensity increase or decrease is visible. A stable Q^4 peak around -85/-87 ppm is visible.

Figure 7. The 1D ^{17}O MAS NMR spectra of titanium-bearing sodium aluminosilicate glasses at 9.4 T with varying XTi [$(Na_{0.5}Al_{0.5-x}Ti_x)$ SiO2] as given in the figure. The spectra showing an increasing fraction of BO(Si-O-Si and Ti-O-Si) with increasing Ti content.

Figure 8. ^{17}O 3QMAS NMR spectra for Ti-bearing sodium aluminosilicate glass in two dimensions; the MAS dimension and Isotropic dimension. With increasing Ti, similarly to MAS spectrum alone, it can be observed that a new peak appears representing Ti-O-Si bonds. The big difference from the 1D and 2D spectra is that the Al-O-Al Na-O-Si and Si-O-Si bonds appear as separate peaks that are distinguishable in the isotropic dimension. The spectra were obtained at 9.4 T with varying XTi [$(Na_{0.5}Al_{0.5-x}Ti_x)$ SiO2]. The contour lines range from 3% to 13% and 13% to 83% relative intensity with increments of 2% and 5% respectively. For x = 0.125 a contour line of 1% is used instead of 83% to better visualize the presence of a small Ti-O-Ti peak.

Figure 9. The 1D ^{27}Al NMR spectra of Ti-bearing sodium aluminosilicate glass with varying XTi [$(Na_{0.5}Al_{0.5-x}Ti_x)$ SiO2]; the MAS dimension and Isotropic dimension are shown in figures a and b respectively. The peak width is getting narrower in both the MAS and isotropic dimension.

Figure 10. The 2D ^{27}Al 3QMAS NMR spectra of Ti-bearing sodium aluminosilicate glass with varying XTi [$(Na_{0.5}Al_{0.5-x}Ti_x)$ SiO2] in two dimensions; the MAS dimension and Isotropic dimension. With increasing Ti, no new peaks are appearing. The only peak visible, related to the O-Al-O bonds, is decreasing in intensity and size with increasing Ti. The peak width is getting narrower in both the MAS and isotropic dimension. The contour lines range from 3% to 13% and 13% to 83% relative intensity with increments of 2% and 5% respectively.

Figure 11. Gaussian fitting of ^{29}Si MAS spectra of Ti-bearing sodium trisilicate glasses. It is assumed that three peaks are present in the glass: Q^2, Q^3 and Q^4.

Figure 12. Peak position and peak width (a and b respectively) plotted against increasing Ti content in the sodium trisilicate glasses.

Figure 13. ^{29}Si MAS NMR spectra for NS_4 (a) and NS_8 (b) glass with increasing Ti content up to 15.0 mol% Ti (Ackerson et al. 2020). In figure c the NS_3 sample from this study is compared to both NS_4 and NS_8 from figures a and b.

List of tables

Table 1. The synthesized Ti-bearing sodium trisilicate glasses (sample set 1) with their corresponding nominal compositions and melting temperature.

Table 2. The synthesized Ti-bearing sodium aluminosilicate glasses (sample set 2) with their corresponding nominal compositions and melting temperature.

Appendix

Appendix A. Lunar glass compositions

Appendix B. Schematic figure of the internal structure of the Moon (Wieczorek 2006).

Appendix C. P and S wave velocity models of the lunar mantle. The model is based on the non-linear Bayesian inversion of (Khan et al. 2014).

Appendix D. Thermal structure of the lunar interior (Khan et al. 2014).

Appendix E. Phase diagram of SiO2 TiO2 and Na2O. The SiO2 concentration is fixed at 75% while TiO2 increases and Na2O decreases. Modified from: (Ackerson et al. 2020) and (Glasser and Marr 1979).

Appendix F. Attended classes

Appendix G. Conference List

1. Introduction

There are many different reasons why a broad interest is shown in the field of glass science. Some might only find their interest in the physical properties of various glasses as there are plenty of technological applications for either commercial, medical, or engineering purposes. However, from a geological perspective, glass is a very important material of which its physical and chemical properties could provide interesting new geological insights. The atomic structure of glass represents the non-crystalline phases for many different kinds of geological compositions. Hence, the atomic structure of glass materials could provide crucial information in order to learn more about the interior of the Earth and other planetary bodies.

1.1. Understanding the lunar interior

The Moon, which is the nearest planetary object to Earth and our only natural satellite, orbits the planet at an average distance of 385,000 km. Since the Apollo 11 mission in 1969, extra-terrestrial exploration began, during which the first lunar rock samples were brought to Earth. For the first time, geologists were able to perform detailed studies on the mineralogy of the Moon. Picritic glasses found in the volcanic products show that partial melting of a heterogeneous mantle is most likely the cause of the mare

volcanics. These picritic glasses are used as the fundamental foundation for interpreting the composition of the deep lunar interior (Ridley et al. 1973); (Heiken 1975); (Delano 1979); (Sato 1979); (Fogel and Rutherford 1995); (Elkins-Tanton, Chatterjee and Grove 2003) and therefore also the lunar mantle evolution.

Composition

The composition of these glasses is given in Appendix A. Most of the component make up a similar fraction among the different glasses except for TiO_2. It is quite noticeable that the Ti content in these lunar glasses varies significantly, ranging from 0.26 wt% to 16.4 wt%. These glasses have been thoroughly studied but still continue to raise some questions about their origin and presence on the lunar surface (Rai et al. 2019, Vander Kaaden, Agee and McCubbin 2015, Wagner and Grove 1997). It is widely believed that the lunar mantle overturn model allows melts from deep inside the lunar interior to ascent to the surface (Delano 1986); (Shearer et al. 2006). The mantle source regions are thought to be depleted in volatile, alkali and siderophile elements. There also seems to be a complete absence of water and hydrous phase.

Lunar evolution

The lunar mantle was formed around 4.5 billion years ago. It is widely believed that a significant differentiation event happened where the magma ocean started to form different crystalline layers (Warren 1985). This partitioning of the mantle is the effect of crystallization and then separation of the melt and the newly formed crystalline material, creating differences in density. This process of mantle crystallization causes the denser material to descent to the lower mantle. These were expected to be Mg-rich olivines and pyroxenes. It is thought that they now form a mafic base of the lunar mantle. Lighter crystals like plagioclase crystallized and form the anorthositic crust of the Moon. Later, other elements also started forming layers; for example, Fe and Ti forming ilmenite in the shallow part of the mantle. A wide variety of other elements remained in the liquid mantle for longer because they are considered to be incompatible elements. These eventually found their place in the last cumulates of the Moon which enriched these layers with ur-KREEP (Potassium, Rare Earth Elements and Phosphorous) (Wagner and Grove 1997). To visualize this lunar mantle evolution, a schematic illustration is provided (figure 1).

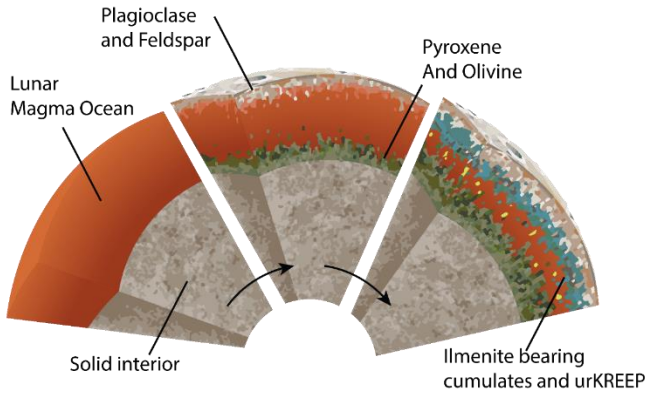

Figure 1. Schematic illustration that represents the lunar magma ocean evolution (E. El Ghazaoui, 2021)

Structure of the lunar Interior

The Moon has a radius of 1737.5 km which makes it about 27% the size of the Earth (radius 6371 km). Similar to investigating Earth's interior, the most important way of obtaining structural information of the lunar interior is seismology. The seismometers sent by NASA were able to record around 1743 meteoroid impacts, 28 shallow- and 7245 deep moonquakes (Nakamura, Latham and Dorman 1982). The largest shallow moonquakes have a magnitude of about 5 and are considered small compared to what we experience here on Earth. For the deep moonquakes the magnitudes are generally around 3 (Goins, Dainty and Toksöz 1981). A schematic figure of the lunar interior is provided in Appendix B.

Crust

From the Apollo 12 and 14 seismic data that was revised(Lognonné, Gagnepain-Beyneix and Chenet 2003), it can be assumed that the base of the anorthositic crust can be found at a depth of 30 to 45 km. This is much thinner compared to what was previously believed to be the base of the crust (60-70 km). The P and S wave velocities increase with depth until around 30 to 45 km depending on the location in the lunar surface. From this depth onward the P and S wave velocities do no change as much as it did in the crust. Until a depth of 1200 km up to 1400 km the P and S wave velocities drop drastically most likely indicating the transition from the lower mantle to the partial melt layer and eventually the liquid outer core Appendix C (Khan et al. 2014) (Weber et al. 2011).

Based on gravity and topography dataset analyses, it can be concluded that the crust is homogeneous in composition. However, when considering remote-sensing constraints this is too simplistic. To satisfy both remote sensing and geophysical constraints, a lunar crust separated into an anorthositic upper crust and noritic lower crust model is being considered (Wieczorek 2006).

Mantle

As direct samples of the mantle have never been identified and remote sensing is no option either, determining the mantle composition can be quite challenging. This deems it necessary to use more indirect methods in order to constrain the mantle composition. These methods are chemical analyses of volcanic glasses and mare basalts, and seismic data. Mare basalts and volcanic glasses are classified based on their TiO_2 concentrations(very low Ti: <1 wt%, intermediate Ti: 1-4 wt% and high Ti: > 8 wt%,). These mare basalts function as a probe for mantle composition, structure, dynamics, and thermal history of the Moon. The composition and depth of the source regions for mare basalts have been tied to models of lunar differentiation (i.e., the lunar magma ocean) and post-LMO mantle dynamics (cumulate overturn and assimilation).

A three-layer lunar mantle was suggested by (Nakamura et al. 1982). These layers range from 58-270 km, 270-500 km, and below 500 km. (Kuskov and Kronrod 1998) used seismic velocities obtained from a thermodynamic model that is based on the velocity profiles from (Nakamura et al. 1982). In their study they suggest that the 58-270 km layer mainly exists of 95 mol% orthopyroxene and 4 mol% clinopyroxene, the 270-500 km layer exists of 92 mol% orthopyroxene, 4 mol% clinopyroxene, 4 mol% olivine and 1 mol% garnet. Below 500 km depth, the compositions are thought to be 56 mol%

olivine, 35 mol% clinopyroxene and 9 mol% garnet. In a similar study by (Khan et al. 2007), where they instead used the arrival time velocity data from (Lognonné et al. 2003), it was assumed that the Moon consists of a crust with a variable thickness but constant composition, an upper mantle and a lower mantle with a upper-lower mantle boundary at 600 km depth. They found that the upper mantle should consists of mainly orthopyroxene (75 wt%) and unconstrained amounts of clinopyroxene olivine and either plagioclase or garnet depending on the depth. Up to a depth of 200 km mostly plagioclase (10 wt%) and up to 600 km garnet(15 wt%). In the lower mantle (below 600 km), the mantle consists of 60 wt% olivine and 40 wt% garnet. The biggest and perhaps most important difference between these the different studies is that in the latter one, they suggest about 40 wt% of garnet whereas the former study only estimate this value to be 9 mol%. This is important as in the model from (Khan et al. 2007) they predict that there is about twice as much aluminium in the lower mantle of the Moon.

What both of these studies neglect in their models is the likeliness of titanium-rich phases present in the mantle due to the suggested lunar mantle overturn model. Even in a more recent study where they do consider titanium to be present in the mantle, it is only being fixed at chondritic values (Kuskov, Kronrod and Hood 2002). Especially at the near-side of the Moon where most if the velocity data originates from in the first place and where hight-Ti

basalts are commonly found, it is important that titanium-rich phases are being included. The reason for this is that the presence of titanium-rich phases could affect the thermodynamic mineral stability fields. Also it could have effects on the composition interpretations based on the seismic velocity model (Wieczorek 2006). As it is still to be determined if this effect is significant or not, research on Ti-rich melt properties could contribute to better understanding its significance.

The maximum melting depth of the lunar magma ocean is thought to be between 500 and 600 km below the lunar surface. This is based on an observed seismic discontinuity at this depth (Khan et al. 2007, Wieczorek 2006). This discontinuity is most likely the case of a change in composition. Despite the initial depth of the lunar mantle, thermal considerations and isotopic evidence are suggesting that lunar mantle crystallized within a time period of 30 million years (Lee et al. 2002); (Righter and Shearer 2003) or 200 million years (Solomon and Longhi 1977).

Core

The core its radius is thought to be between 310-380 km and has an estimated density of 5.2-6.7 g/cm^3 (Morard et al. 2018). The composition of the lunar core is still not well constrained. It might consist of a Fe-FeS-C

metallic alloy or even molten silicate materials enriched in iron and titanium to account for the larger density (Wieczorek 2006).

Temperature

The average temperature in the lunar magma ocean is thought to be around 1400 K(1127 °C) according to (Maurice et al. 2020). Based on the study by (Khan et al. 2014) it shows that the temperature gradient in the lunar mantle ranges from 0.5 to 0.6 °C/km with reaching temperatures around 1600-1800 °C at the partial melt layer at the bottom of the mantle(1300 km). In the lunar crust this temperature gradient is much steeper. In Appendix D the lunar temperature profile of the mantle is shown directly from (Khan et al. 2014). The bright yellow line represents the solidus for peridotite (Hirschmann 2000). Two other models by (Longhi 2006) and (Taylor 1982) representing the Lunar Primitive Upper Mantle(LPUM) and Taylor Whole Moon(TWM) compositions. It can be observed that around 1100 km in depth, the lunar geotherm or crossed these solidi. This suggests that melting in the lower parts of the mantle is possible. Comparing this to the seismic data it is also in agreement as there is a sharp decrease in S wave- and also a drop in P wave velocities around this depth.

1.2. Effects of Ti on the structure of glasses

Plenty of knowledge is available from previous studies about what the effects are of titanium on the physical properties of non-crystalline materials. However, the role that titanium plays in lunar melts and therefore the way this could contributes to constraining the evolution of the Lunar magma ocean, is not yet thoroughly investigated. In other words, what is not really known yet is how the structural observations from lunar glasses can be linked to the macroscopic physical- and thermodynamical properties. The main purpose of this study is to use the structural data of Ti bearing sodium trisilicate- and sodium aluminosilicate glasses obtained with Nuclear Magnetic Resonance(NMR) spectroscopy, to better understand the lunar magma ocean evolution.

By studying the effect of Ti in sodium aluminosilicate glass or nepheline($NaAlSiO_4$), Ti is usually a network former but can also be a network modifier depending on the coordination number (Nienhuis et al. 2020). It was found that $^{[4]}$Ti is a network former while on the other hand $^{[6]}$Ti is a network modifier (Mysen and Neuville 1995). In Ti bearing silicate glasses the Ti atom is mostly incorporated as $^{[5]}$Ti. This $^{[5]}$Ti can function as both network modifier and network former simultaneously as the Ti atom may bond with one nonbridging oxygen and four bridging oxygen atoms. The nonbridging oxygen atom then forms a short double bond with the Ti atom.

[4]Ti was observed as the dominant coordination for low Ti-bearing glasses(< 3wt% TiO_2). Thus, increasing the Ti content shifts to substantially more [5]Ti in the silicate glass. [6]Ti seems to be only a very minor part within the sodium silicate glass, but this might increase under high pressure conditions. (Farges et al. 1996a, Farges and Brown 1997, Farges et al. 1996b, Farges, Brown and Rehr 1996c, Farges, Brown and Rehr 1997).

One of the more obvious properties that seems to be affected by an increase in Ti content is the density. When TiO_2 was added to phosphate-based glass, the density of this material increases significantly from 2.63 cm^{-3} to 2.74 cm^{-3} from 0 mol% to 15 mol% respectively (Kiani et al. 2010). As a density increase is to be predicted when it substitutes other elements in the glass network, simply because Ti has a relatively larger mass than other elements (Si, Al, Mg or Na), it is much more interesting to look at the compressibility of Ti bearing glasses as this shows the change in density with applied pressure. Besides these density measurements, interesting observations were made on the compressibility of Ti bearing lunar glass (Vander Kaaden et al. 2015). In this study, the compressibility can be expressed as the change in density per pressure applied to the sample. Initially, an increasing density of 0.17 g/cm^3/GPa was observed. However, after 8 GPa the data shows that the compressibility decreases with 0.09 g/cm^3/GPa.

When the glass composition, pressure, or temperature of a sample changes, it affects other properties of this glass significantly. Viscosity is one of these properties and has been shown to increase with increasing pressure of the melt and thus also with increasing polymerization (Wang et al. 2014). In this study polymerization is described as the ratio of non-bridging oxygen (NBO) divided by the number of Network formers (NF). If NBO/NF ≥ 2, it is considered a depolymerized melt and when NBO/NF ≤ 1 it is considered a polymerized melt. In some cases when the pressure increases that is applied on a melt, the viscosity decreases. For a depolymerized Di sample (diopside) the pressure was increased from 8.5 to 13 GPa and the viscosity decreased (Reid et al. 2003). This shows that viscosity plays a very important role in the mantle of the moon for example. If the viscosity of a melt with a certain composition suddenly starts to increase because of increasing pressure in the mantle with depth, it might have significant consequences on the diffusivity and thermodynamical properties of the melt.

By extending the knowledge about the Ti coordination of lunar melts, some crucial insights could be obtained to better understand the cumulation events and high Ti bearing melts in the lunar magma oceans during the Hadean as (Wagner and Grove 1997) carefully evaluated with several different models.

The components that form the glass in this research are TiO_2 ,Na_2O, and SiO_2(Ti-bearing sodium trisilicate glass and Ti-bearing sodium metasilicate) and TiO_2 ,Na_2O, Al_2O_3, and SiO_2 (Ti-bearing sodium aluminosilicate glass). These is a relatively simple composition and are meant to purely observe how Ti will affect the glass structures. It is the intention to set up a sturdy foundation of structural knowledge before moving towards the more realistic compositions. The Ti-bearing trisilicate glasses represent the simplest model where the aluminosilicate glasses are slightly more complex.

In (Ackerson et al. 2020) similar experiments have been conducted as in this research. They synthesized Na-silicate glasses and studied the influence that Ti has on the structure of this amorphous material. NS4 and NS8 glasses were made while in this study NS3 is used. From the results it is assumed that Ti is incorporated as $^{[5]}Ti$ and that there is no interaction between Ti and Na visible unlike what was found in previous studies where Ti tends to cluster with Na making Na-titanite (Farges et al. 1996a, Yarker et al. 1986).

Alkali oxides like N_2O are well known to be incorporated into the silicate glass network and increase the amount of non-bridging oxygen. The glass becomes less polymerized and therefore the structure of the glass will change. It is generally assumed that Al and Si are good network formers. Because Al has a charge of Al^{3+}, the system has to be charge balanced by a metal cation. In the case of this study Na^+ ions are used. Depending on the composition of

the glass, the excess Na^+ ions that are not used for charge balancing, are assumed to break up the aluminosilicate network as more non-bridging oxygen (NBO) bonds are forming within the system. In an earlier study(Grillo and Carrazza 1997), using lattice energy minimization (LEM) and quantum chemical calculations, it has been observed that Al-O-Si-O-Ti bonds are preferential over Al-O-Ti bonds. This suggests a clear Al, Ti avoidance. In the study by (Lee 2004), it was also found that under high pressure conditions the coordination state of atoms can change. This was observed for by using NMR spectroscopy for sodium silicate- and aluminosilicate glasses. The $^{[4]}$Al changed into $^{[5]}$Al and eventually $^{[6]}$Al with increasing pressure. Also, it was shown that with increasing pressure, the fraction of nonbridging oxygen(Na-O-Si) decreased resulting in a polymerization of the melt. As Ti can also take the form of $^{[4]}$Ti, $^{[5]}$Ti and $^{[6]}$Ti, it is quite likely that incorporation of Ti in the lunar mantle materials is affected by the pressure. In this study the experiments are performed at 1 atm pressure. In future studies it would be interesting to see how applying high pressure could affect the structure of Ti-bearing glasses.

In this study the effects of Ti on the network polymerization in Ti-bearing sodium silicate- and aluminosilicate glasses were studied using ^{29}Si, ^{17}O and ^{27}Al NMR spectroscopy. Also some quantum chemical calculations have been performed in order to compare this with the NMR data. In the following

section, the experimental methods are described in detail(how the samples are synthesized, information regarding the NMR experiments, and how the quantum chemical calculations were performed). The experimental NMR results are provided and thoroughly analysed right after. It is than later discussed and compared with the calculations done in this study. The implications for lunar mantle dynamics are also discussed in this section before concluding the most important finding from this research.

2. Experimental methods

2.1. Sample composition

Three major components were used for the synthesis of the samples that are used in this study. Rutile (Sigma Aldrich) for TiO_2, white quartz (Sigma Aldrich) for SiO_2, Sodium carbonate (ACS reagent Sigma Aldrich) for Na_2CO_3 and aluminium oxide(Sigma Aldrich) for Al_2O_3. The components are ground together in an agate mortar and pestle in order to have a fine-grained mixture of these components. A 0.2 wt% of Cobalt(II) oxide(Sigma Aldrich) CoO is added as well in order to reduce the relaxation time of the nuclei in the magnetic field, which shortens the overall duration of the NMR experiments. This is especially useful for ^{29}Si NMR experiments as the Si nuclei has a long relaxation time.

Two sets of samples have been synthesized with varying compositions. The compositions of the samples per set are shown in table 1 and table 2. A total of 100 mg was synthesized per sample. The first set consists of Ti-bearing sodium trisilicate glasses. A few of these are synthesized with 40% ^{17}O enriched SiO_2. Set 1 consists of samples with increasing TiO_2 content only at the expense of Na_2O content of the samples. Substituting Ti (network former), for Na(network former) only, will provide better structural information for Ti incorporation in silicate melts.

The second set includes Al_2O_3 forming Ti-bearing sodium aluminosilicate glasses and instead of using trisilicate, metasilicate is used. This increases the of Ti/Si ratio and therefore more drastic changes in the NMR results are expected. The Na content in these glasses remains the same. This second set differs from the first by the fact that one network former is substituted with another(Al with Ti).

Table 1. The synthesized Ti-bearing sodium trisilicate glasses (sample set 1) with their corresponding nominal compositions and melting temperature.

Sample set 1 Composition **Ti-bearing Sodium trisilicate glass ($Na_{(1-x)}$: Ti_x : 3 SiO_2)**		Oxides (mol%) Nominal			Melting temperature (°C)
x		SiO_2	Na_2O	TiO_2	
0	$NaSiO_2$	75	25	0	1100
0.10*	$(Na_{0.90}\ Ti_{0.10})$: 3 Si	75	22.5	2.5	1200
0.20	$(Na_{0.80}\ Ti_{0.20})$: 3 Si	75	20	5	1250
0.25*	$(Na_{0.75}\ Ti_{0.25})$: 3 Si	75	18.75	6.25	1300
0.33	$(Na_{0.67}\ Ti_{0.33})$: 3 Si	75	16.75	8.25	1400
0.40	$(Na_{0.60}\ Ti_{0.40})$: 3 Si	75	15	10	1450
0.50*	$(Na_{0.50}\ Ti_{0.50})$: 3 Si	75	12.5	12.5	1550
0.67	$(Na_{0.33}\ Ti_{0.67})$: 3 Si	75	8.25	16.75	1600
0.75*	$(Na_{0.25}\ Ti_{0.75})$: 3 Si	75	6.25	18.75	1650

* ^{17}O-enriched sample

Table 2. The synthesized Ti-bearing sodium aluminosilicate glasses (sample set 2) with their corresponding nominal compositions and melting temperature.

Sample set 2 Composition **Ti-bearing Sodium aluminosilicate glass ($Na_{0.5}$: $Al_{(0.5-x)}$: Ti_x : SiO_2)**		Oxides (mol%) Nominal				Melting temperature (°C)
x		SiO_2	Na_2O	TiO_2	Al_2O_3	
0*	$NaAlSiO_4$ (Nepheline)	50	25	0	25	1600
0.125*	$Na_{0.5}$: $(Al_{0.375}\ Ti_{0.125})$: Si	50	25	6.25	18.75	1600
0.25*	$Na_{0.5}$: $(Al_{0.25}\ Ti_{0.25})$: Si	50	25	12.5	12.5	1600
0.375*	$Na_{0.5}$: $(Al_{0.125}\ Ti_{0.375})$: Si	50	25	18.75	6.25	1600
0.50*	$NaTiSiO_7$	0	25	25	0	1600

* ^{17}O-enriched sample

2.2. Heating and quenching

The samples used in this study were heated in a platinum crucible with a maximum volume of 5 cm^3. They were synthesized at various temperatures depending on their composition (table 1 and 2). The melting temperatures for

the samples of set 1 are determined based of the ternary phase diagram of the components Na_2O, SiO_2 and TiO_2 (Appendix E). Melting temperatures for the aluminosilicate glasses were constant for every composition (1600). The quenching process of the crucible containing the sample is done manually. The quenching should be done in just a few seconds. Within this short duration out of the furnace, the crucible has time to cool down from the desired temperature. For this reason, the samples are heated up to the melting temperatures derived from the phase diagram plus an additional 200-250 °C, to prevent unwanted crystallization from happening while out of the furnace(set 1).

Because $NaCO_3$ is used, decarbonation of the samples is necessary. When the samples reached 800 °C, they were kept at this temperature for 30 minutes to completely decarbonize the sample. Some Na loss should also be considered. Because of the relatively high melting temperatures and the decarbonation process, Na loss might change the final composition of the samples. Therefore, ICP-AES analyses should be performed in order to determine this final sample composition.

Evidence of the incorporation of Ti into platinum has not clearly been confirmed or refuted in earlier studies. According to the size of Ti atoms it is unlikely that it will happen as they are bigger than Pt atoms. To reassure this from happening nonetheless, the crucible used for these samples was

preconditioned with two 10 mol% Ti samples. ICP-AES data for these two samples show that there is no loss of Ti as the values are almost identical to one another.

After quenching, the bottom of the crucible is deformed by hand in order to separate the synthesized glass from the platinum crucible. The glass chunks are then ground in the mortar until a very fine-grained powder remains. Fine powder is preferential for NMR rotor spinning as this will reduce the mass difference inside the rotor. The colour of the glass is supposed to be blue, and it varies between light blue and dark blue depending on the added amount of CoO. After grinding the sample, it is kept in a vial inside a desiccator until further use Some hygroscopic samples were handles in a glovebox under Ar gas conditions. The crucible is cleaned by heating it up for 15 minutes over a flame with Na_2CO_3 inside. The remnants of the glass will be mixed with the Na_2CO_3 which can then later be dissolved using water. The smaller invisible parts will be chemically removed by boiling the crucible for 15 minutes in ionized water. At last, it was cleaned with ethanol for future use.

2.3. XRD analyses

Based on previous studies (Nienhuis et al. 2020) it can be expected that the amount of Ti added to the glass is limited due to the potential crystallization

of TiO_2 within the glass in the form of either rutile or anatase. In this paper it is stated that for samples with Ti content exceeding 15 mol%, a crystallized layer made of TiO_2 on top of the glass and a ceramic-like material was observed. In this study however, samples were synthesized containing up to 16.75 mol% and 18.75 mol% Ti (set 1). For the sample containing 18.75 mol% Ti, XRD analysis was performed in order to ensure that the samples solely consist of NTS_3 glass. A small amount of glass powder is required to do the X-ray diffraction spectroscopy experiments. The XRD spectra for rutile, a stable phase of TiO_2 at atmospheric pressure, is used as reference for any possible crystalline TiO_2 present in the glasses. As can be seen in figure 2, the signal for NTS_3 glass does not have any peaks. The spectrum for Rutile shows clear peaks.

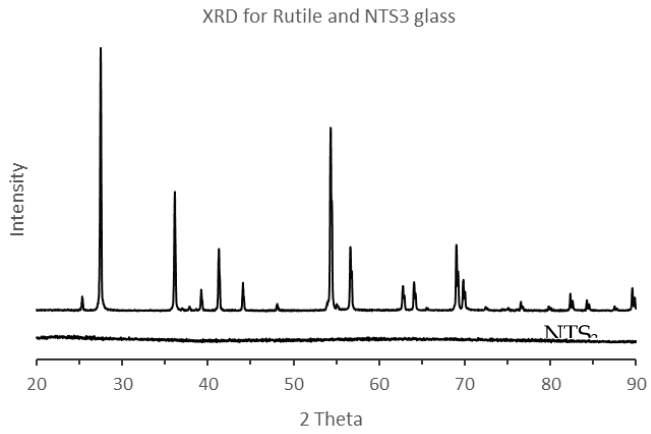

Figure 2. X-ray diffraction spectra for rutile and NTS_3 glass containing 18.75 mol% Ti. No clear peak is visible in the glass sample meaning that there is no crystalline material present. Despite having a high Ti concentration, the synthesis was successful.

2.4. NMR Spectroscopy

Both ^{29}Si and ^{17}O solid-state NMR experiments were conducted for the Ti-bearing sodium trisilicate glass samples. Combining the collective knowledge obtained from these two different NMR methods might be very important to find structural information that otherwise could have been overlooked.

The ^{29}Si solid-state NMR experiments were conducted by using a Varian spectrometer (400 MHz, 9.4 T). The fine-grained samples placed in a 4 mm zirconia (ZrO_2) rotor with long caps were inserted in the Doty 4mm probe. The reference sample of SiO_2 called tetramethylsilane or TMS was used to calibrate the machine for the ^{29}Si signal at a Larmor frequency of 79.47 MHz. The bearing pressure and driving pressure causing the rotor to rotate, were manually set to 30.2 psi and 18-19 psi respectively. The spinning speed for these samples is 14 kHz. Because of the long relaxation time for ^{29}Si, every experiment took at least 4 days.

^{17}O NMR and ^{27}Al NMR experiments were performed using the same Varian spectrometer (400 MHz, 9.4 T). This time however, a double resonance probe with 3.2 mm rotor setup was used. The Larmor frequency for ^{17}O NMR is 54.23 MHz and the reference material used in this case is H_2O. For the ^{27}Al NMR experiments the Larmor frequency is 104.23 MHz. For referencing liquid aluminium chloride ($AlCl_3$) was used.

Data from both magic angle spinning(MAS) and triple quantum magic angle spinning(3QMAS) NMR experiments were collected with a spinning speed of 17 kHz for the ^{17}O NMR and 18 kHz for ^{27}Al NMR experiments.

3. Results

3.1. Ti-bearing sodium trisilicate glasses

^{29}Si NMR Spectroscopy

In figure 3, ^{29}Si NMR data are shown for the Ti-bearing sodium trisilicates. The ^{29}Si NMR spectra provide Q^n species information where n is the number of Bridging Oxygen(BO) of a single Si tetrahedron. Thus, the glass is more polymerized when Q^n has a higher number. Two peaks are clearly shown for the NS_3 endmember(Ti = 0); one peak around -90 ppm representing the Q^3 species and another peak around -104 ppm representing Q^4 species.

Without any Ti present in the sample, the Q^3 species are more dominant within the sample. However, when Ti is incorporated at the expense of Na, the Q^3 species fractionation will decrease. Because the spectra are normalized to their maximum value, this decrease might be overlooked for the low Ti samples. Reaching high Ti concentrations, the peak intensity for the Q^4 species become the dominant fraction, indicating a significant change in the network polymerization of the glass. This implies that the network

polymerization is highly dependent on the Ti content as this element seems to act as a network former.

The Q^3 and Q^4 peak positions are shifting towards lower frequencies; (-90 to -95 and -104 to -109). Based on the peak positions of the Q species in the Na trisilicate endmember, a relationship between peak position and Si-O-Si bond angle has been established. The observed peak shifts are most likely due to an increase in Q species that contain more Ti as the next nearest neighbour.

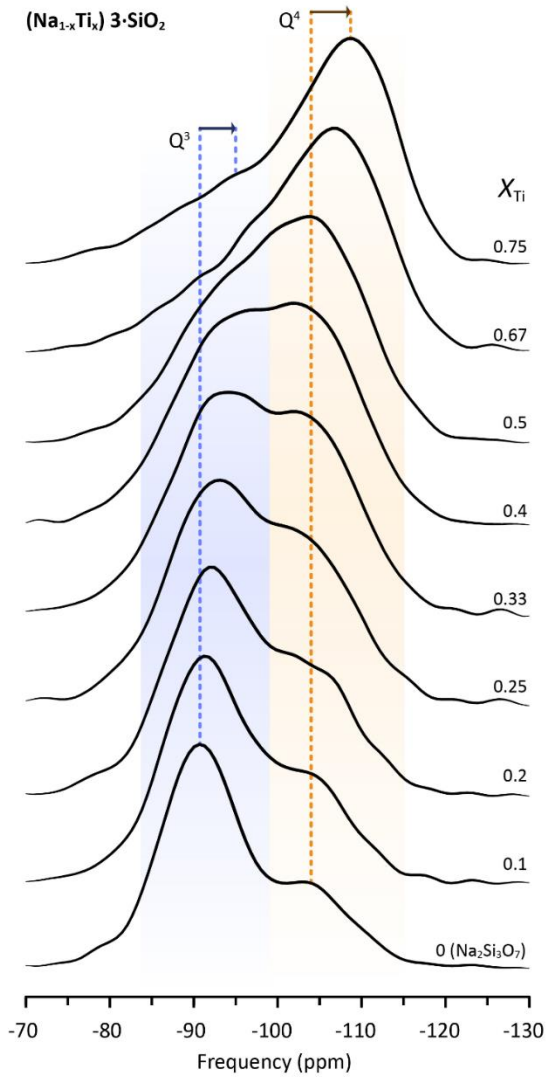

Figure 3. Showing in this figure are the ^{29}Si MAS NMR spectra which shows the effect of substituting Ti for Na in NS_3 glass for the Ti-bearing sodium trisilicate glasses in set 1. A clear peak intensity increase is visible for the Q^4 peak with a frequency of -104 ppm at the cost of the Q^3 peak at -90 ppm. This indicates a change in Q species with increasing Ti content in the samples. Both peaks clearly show a shift towards lower frequencies.

^{17}O NMR Spectroscopy

The information from the ^{29}Si NMR experiments show a clear change in the network polymerization with increasing Ti content. However, the Q^3 and Q^4 peaks overlap with each other which makes it difficult to make a clear distinction between them. The ^{17}O NMR experiments allow us to unveil even more structural information about these Ti bearing Na trisilicate glasses by focussing on the oxygen bonds within five of the samples in set 1 which contain ^{17}O enriched SiO_2(Ti = 0, Ti = 0.1, Ti = 0.25, Ti = 0.5 and Ti = 0.75).

The ^{17}O MAS NMR spectra are shown in figure 4. Just like the endmember (Ti = 0) for the ^{29}Si NMR experiments, the ^{17}O NMR endmember (Ti = 0) shows two overlapping peaks for BO(bridging oxygen) and NBO(non-bridging oxygen). When increasing the Ti content, these peaks do not seem to change that much; especially when comparing to the ^{29}Si NMR spectra. Nevertheless, the ^{17}O NMR spectra provide new information. Around 110 ppm for the sample Ti = 0.1, a very broad and weak signal appears. This signal is more noticeable when magnifying the spectrum(4x). With increasing Ti content, it becomes clearly visible even without magnification as it increases in intensity and becomes broader simultaneously. This signal represents the Ti-O-Si bonds within the glass. What seems to be to the peak of this signal shifts towards higher frequencies(110 to 180 ppm). This is the

opposite direction of the Na-O-Si and Si-O-Si bonds from 30 to 10 ppm and -10 to -25 respectively.

As the Na-O-Si bond and Si-O-Si bond overlap in the MAS spectra, the 3QMAS data shows how these two peaks can be easily distinguished in two dimensions: the previously discussed MAS dimension and the isotropic dimension (figure 5). With increasing Ti content, the peak intensity for Na-O-Si decreases while the Si-O-Si peak increases. Even though this is a similar observation based on data from the ^{29}Si NMR experiments, these different oxygen configurations are now more distinguishable in the isotropic dimension as the quadrupolar coupling effect decreases while using 3QMAS NMR.

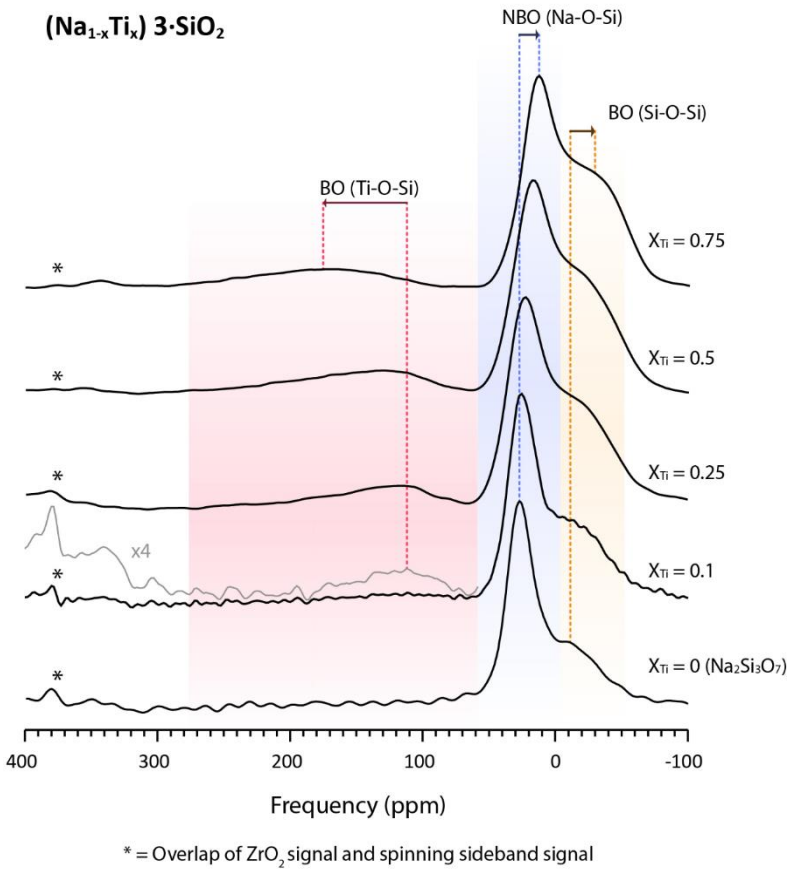

Figure 4. The 2D ^{17}O 3QMAS NMR spectra of titanium-bearing sodium trisilicate glasses at 9.4 T with varying XTi [$(Na_{1-x}Ti_x)$ $3{\cdot}SiO_2$] as given in the figure. The spectra showing an increasing fraction of BO(Si-O-Si and Ti-O-Si) with increasing Ti content. At Ti=0.1 a new broad peak appears around 110 ppm which later increases in intensity and shifts towards higher frequencies. The already existing peaks are both shifting the opposite direction.

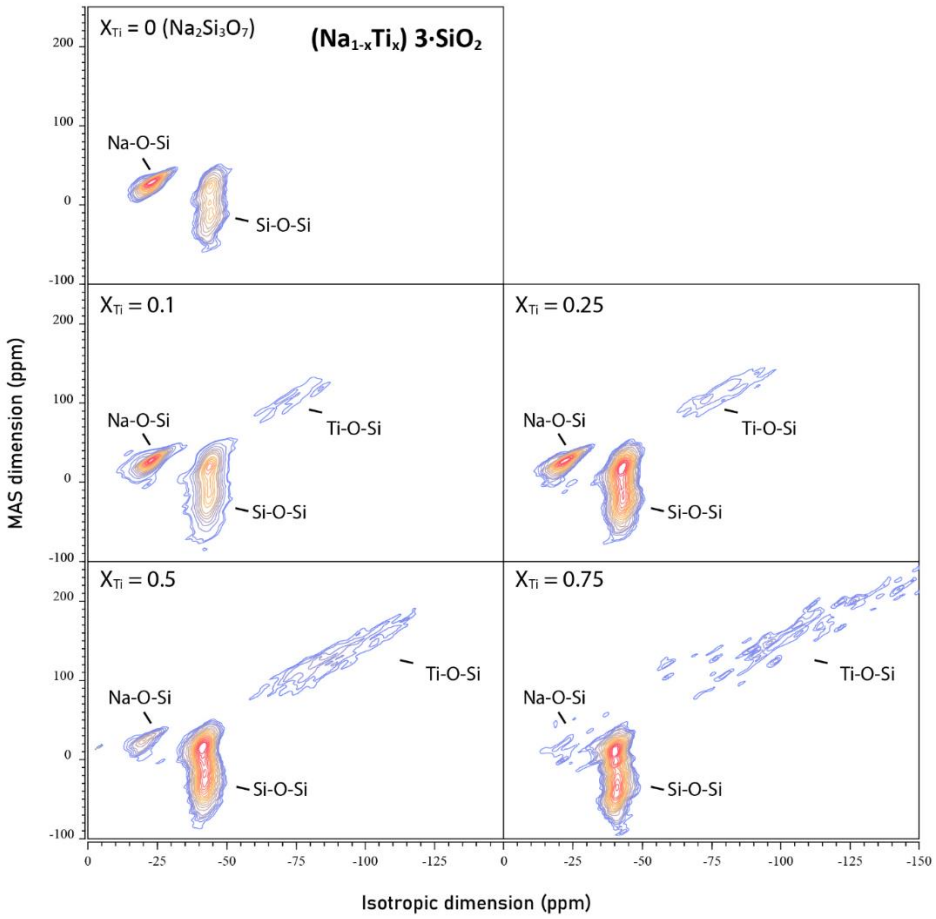

Figure 5. ^{17}O 3QMAS NMR spectra for Ti-bearing sodium trisilicate glass in two dimensions; the MAS dimension and Isotropic dimension. With increasing Ti, similarly to MAS spectrum alone, it can be observed that a new peak appears representing Ti-O-Si bonds. The big difference from the 1D and 2D spectra is that the Na-O-Si bonds and Si-O-Si bonds appear as separate peaks that are distinguishable in the isotropic dimension. The 2D ^{17}O 3QMAS NMR spectra of titanium-bearing sodium trisilicate glasses at 9.4 T with varying XTi [$(Na_{1-x}Ti_x)$ $3{\cdot}SiO_2$] as given in the figure. The contour lines range from 3% to 13% and 13% to 83% relative intensity with increments of 2% and 5% respectively. For x = 0.1, a contour line of 2% is used instead of 83% to better visualize the presence of a small Ti-O-Ti peak.

3.2. Ti-bearing sodium aluminosilicate glasses

^{29}Si NMR Spectroscopy

The ^{29}Si MAS NMR spectra (figure 6) of the sodium aluminosilicate glasses of set 2 show the effect of substituting Ti atoms for Al atoms. Starting from the initial Al-rich composition nepheline, no clear peak intensity changes are visible with increasing Ti content. Around -85/-87 ppm a stable Q^4 peak is present. This indicates that the network is fully polymerized. In this case the sodium atoms function as charge balancing cations. Q species fraction does not chance with increasing Ti content in the samples. The slight change in chemical shift towards lower frequencies might be due to the change in next nearest neighbour for the Si atoms (Al to Ti). The apparent peak shape becomes more asymmetrical with increasing Ti content. This is due to the increase in various Q^4 species. Based on this spectrum alone not much else can be determined.

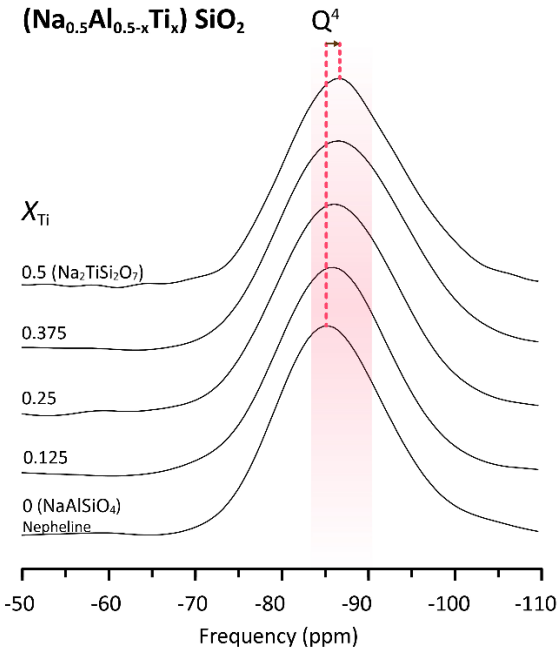

Figure 6. The ^{29}Si MAS NMR spectra show the effect of substituting Ti for Al in sodium aluminosilicate glass of set 2. It starts with the Al-rich endmember also known as nepheline. No clear peak intensity increase or decrease is visible. A stable Q^4 peak around -85/-87 ppm is visible.

^{17}O NMR Spectroscopy

From the ^{17}O NMR spectra of the aluminosilicate samples, a lot of information can be obtained. As the oxygen nuclei are the connection building blocks of the glass, they provide the most detailed information. starting with the endmember nepheline in the MAS NMR spectrum (figure 7), a single symmetric peak clearly stands out with a peak position of 20 ppm. By slowly adding Ti to the system, this peak starts to shift towards higher frequencies and the symmetric shape changes into a more asymmetric on with a more gradual slope on the lower frequency side. This shape is due to the increase in Si-O-Si bonds within the system. The initial peak that was observed in nepheline shifts towards higher frequencies as a result of having less Al-O-Si and more Na-O-Si in the glass. Also, a very low intensity but broad signal appears around 200 ppm. With increasing Ti, this peak becomes much larger, and it does not come as a surprise that this peak is due to the increase of Ti-O-Si bonds within the system.

The peaks described in figure 7, can also be seen on the MAS dimension in the 2D spectra in figure 8. Suddenly peaks become visible in the isotropic dimension. For Ti = 0(nepheline), a clear distinction between Al-O-Al, Al-O-Si- and Si-O-Si peaks can be made. Around the peak for Al-O-Si some overlap is still visible with the nonbridging oxygen bond Na-O-Si. In the Ti

endmember only, this fraction remains around this range. The peak for Al-O-Al slowly disappears as Al is being replaced with Ti which simultaneously causes the large Ti-O-Si peak to appear. In the endmember nepheline mostly Al-O-Si is present indicating that aluminium and silicon are good network formers that like to bond together. As aluminium decreases with increasing Ti content and the Na-O-Si peak is increasing, it could mean that the network becomes less polymerized with increasing Ti content. Although because of the overlap between these bonds, it is hard to tell. The shape of the Na-O-Si peak is more diagonal while the Al-O-Si is more vertical from the isotropic perspective.

As earlier mentioned by the study of (Grillo and Carrazza 1997), Ti nuclei favour to be incorporated with Si atoms as their next nearest neighbour instead of Al. Therefore, there is no clear evidence that an Al-O-Ti peak is present. It could be that there is overlap with another peak, however, this cannot be determined. In order to understand this better, quantum calculations were done in an attempt to find the chemical shielding tensor for the O nuclei between titanium and aluminium.

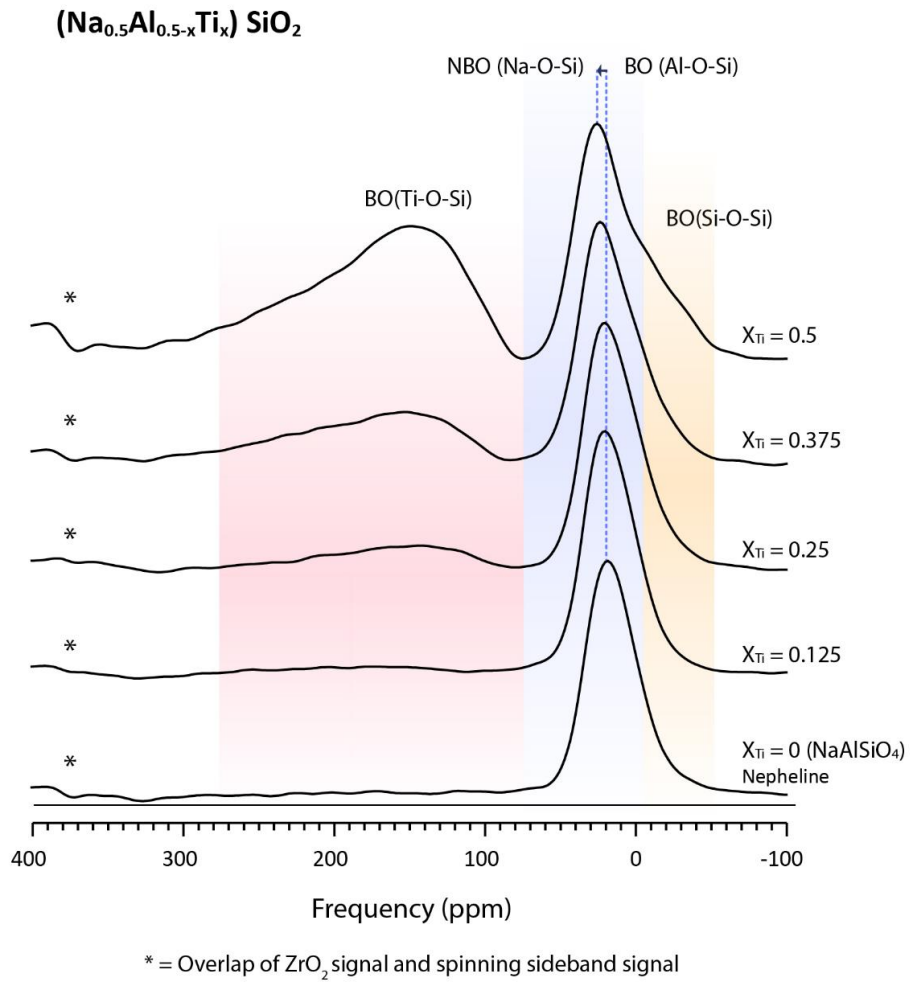

Figure 7. The 1D ^{17}O MAS NMR spectra of titanium-bearing sodium aluminosilicate glasses at 9.4 T with varying XTi [$(Na_{0.5}Al_{0.5-x}Ti_x)$ SiO2] as given in the figure. The spectra showing an increasing fraction of BO(Si-O-Si and Ti-O-Si) with increasing Ti content.

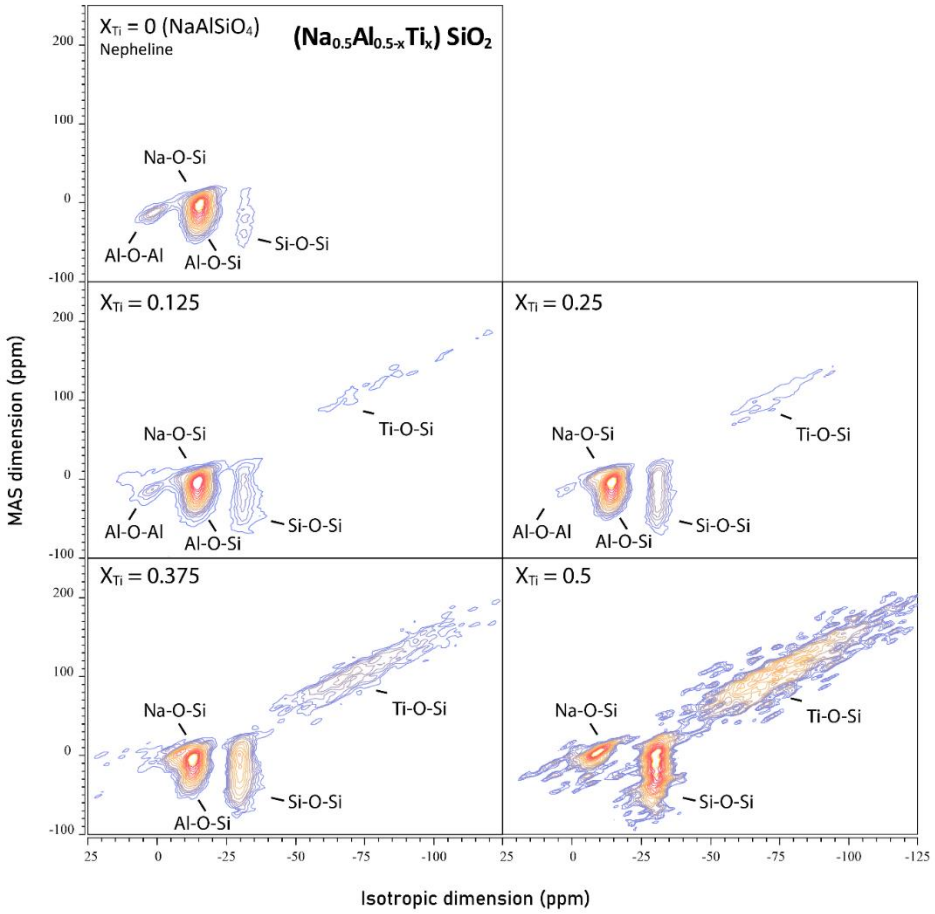

Figure 8. ^{17}O 3QMAS NMR spectra for Ti-bearing sodium aluminosilicate glass in two dimensions; the MAS dimension and Isotropic dimension. With increasing Ti, similarly to MAS spectrum alone, it can be observed that a new peak appears representing Ti-O-Si bonds. The big difference from the 1D and 2D spectra is that the Al-O-Al Na-O-Si and Si-O-Si bonds appear as separate peaks that are distinguishable in the isotropic dimension. The spectra were obtained at 9.4 T with varying XTi [$(Na_{0.5}Al_{0.5-x}Ti_x)$ SiO2]. The contour lines range from 3% to 13% and 13% to 83% relative intensity with increments of 2% and 5% respectively. For x = 0.125 a contour line of 1% is used instead of 83% to better visualize the presence of a small Ti-O-Ti peak.

^{27}Al NMR Spectroscopy

For the ^{27}Al NMR Spectroscopy data both 1D and 2D experiments were performed. In figure 9 both the MAS and Isotropic spectra are shown for the Ti-bearing sodium aluminosilicate glasses. What can be observed from these spectra is that in both dimensions narrowing of the peaks as a result of Ti incorporation occurs. The effect of peak narrowing is a direct consequence of the network becoming more ordered. This sounds counterintuitive as by adding another component to a system, more network disorder could be expected.

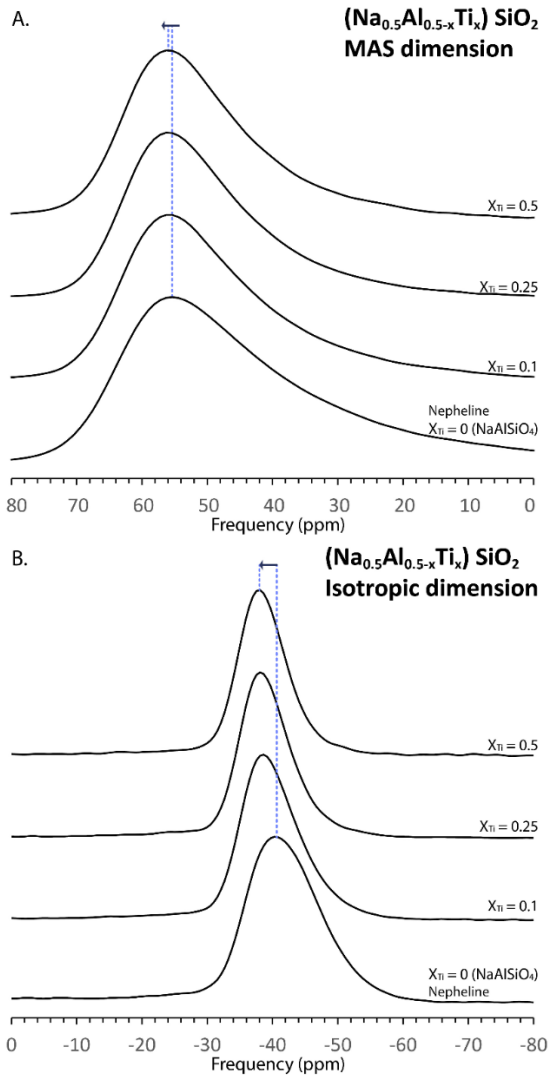

Figure 9. The 1D ^{27}Al NMR spectra of Ti-bearing sodium aluminosilicate glass with varying XTi [$(Na_{0.5}Al_{0.5-x}Ti_x)$ SiO2]; the MAS dimension and Isotropic dimension are shown in figures a and b respectively. The peak width is getting narrower in both the MAS and isotropic dimension.

From the ^{27}Al 3QMAS NMR data it can be seen that the signal becomes narrower in both dimensions too (figure 10). However, this is not as well defined as in the MAS and isotropic dimensions.

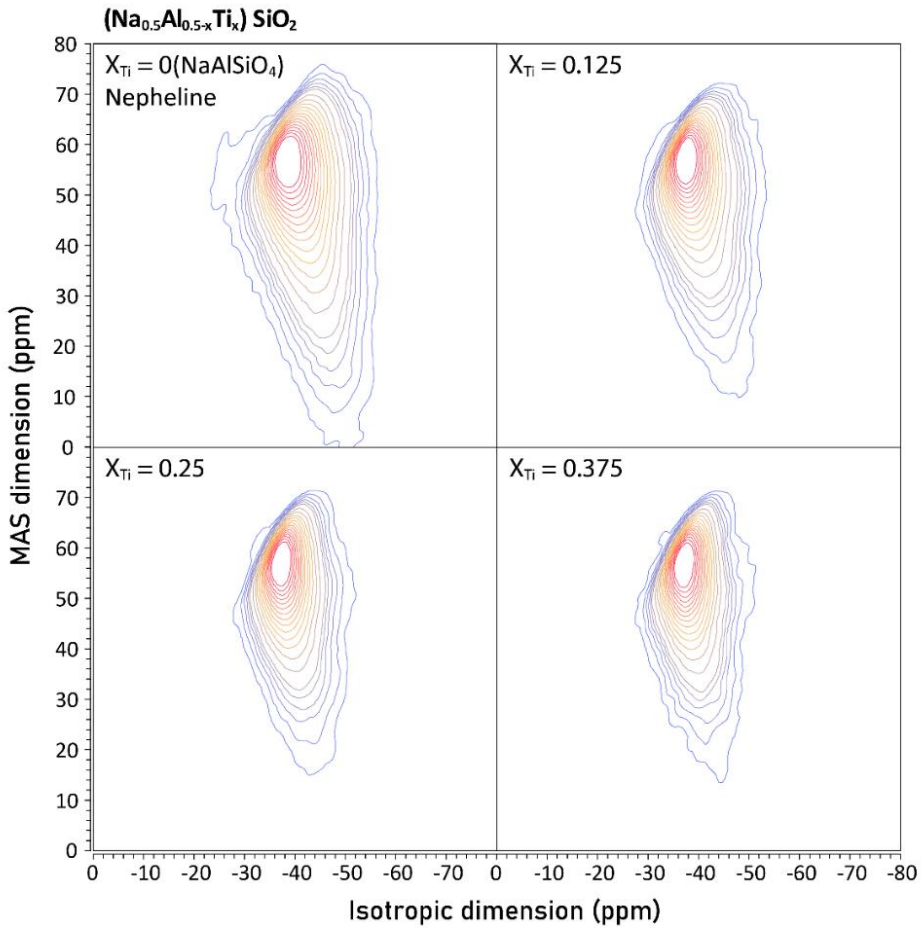

Figure 10. The 2D ^{27}Al 3QMAS NMR spectra of Ti-bearing sodium aluminosilicate glass with varying XTi [$(Na_{0.5}Al_{0.5-x}Ti_x)$ SiO2] in two dimensions; the MAS dimension and Isotropic dimension. With increasing Ti, no new peaks are appearing. The only peak visible, related to the O-Al-O bonds, is decreasing in intensity and size with increasing Ti. The peak width is getting narrower in both the MAS and isotropic dimension. The contour lines range from 3% to 13% and 13% to 83% relative intensity with increments of 2% and 5% respectively.

4. Discussion

4.1. Q species fitting

According to a previous study, the peak positions of the Q species of sodium trisilicate glass was determined to be 78.0, 91.7 and 104.1 ppm for Q^2, Q^3 and Q^4 respectively (Maekawa et al. 1991). These values are used for gaussian fitting in for the ^{29}Si MAS spectra in this study. It is assumed that the gaussian peak for Q^4 increases with increasing Ti content at the expense of Q^2 and Q^3 as the general shape of the spectra seems to change. In figure 11, gaussian fitting was performed with the assumption that the peak positions for these separate Q species would increase. The peak intensity and peak width were unconstrained variables. From the figure it can be seen that the Q^4 species fraction indeed increases in intensity while the other peaks decrease.

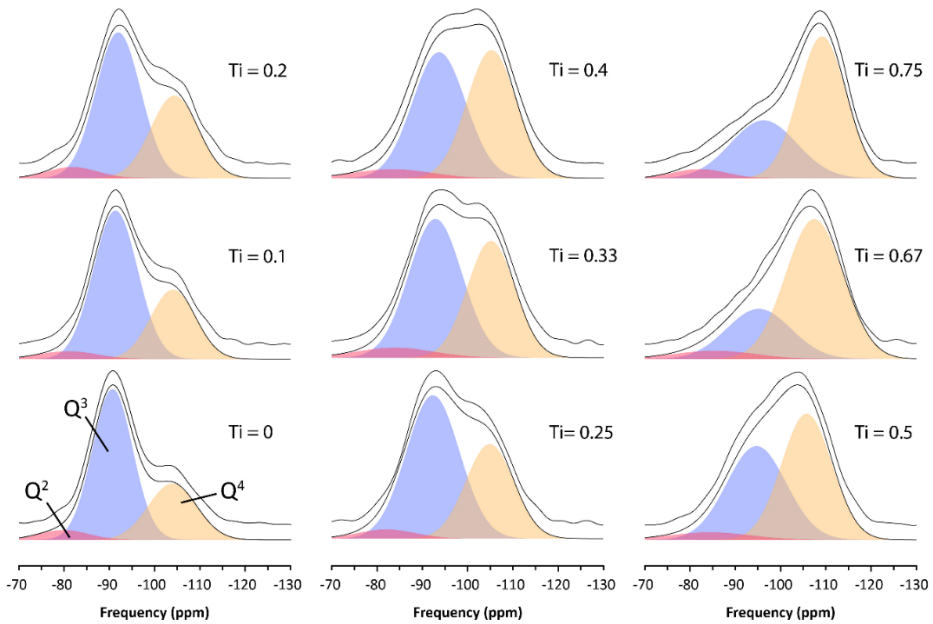

Figure 11. Gaussian fitting of ^{29}Si MAS spectra of Ti-bearing sodium trisilicate glasses. It is assumed that three peaks are present in the glass: Q^2, Q^3 and Q^4.

The peak position and peak width of the fitting data are plotted against the Ti content(figure 12). From these figures it can be seen that the position change with increasing Ti content could be assumed to be linearly increasing. For the peak width no constraints were used therefore the results are quite speculative. It seems like the best fit for the spectra was with a broad Q^3 peak for almost every composition. This peak width seems to increase rapidly for low Ti-bearing glasses and then this increase flattens out when Ti and Na are about equally proportioned in the glass.

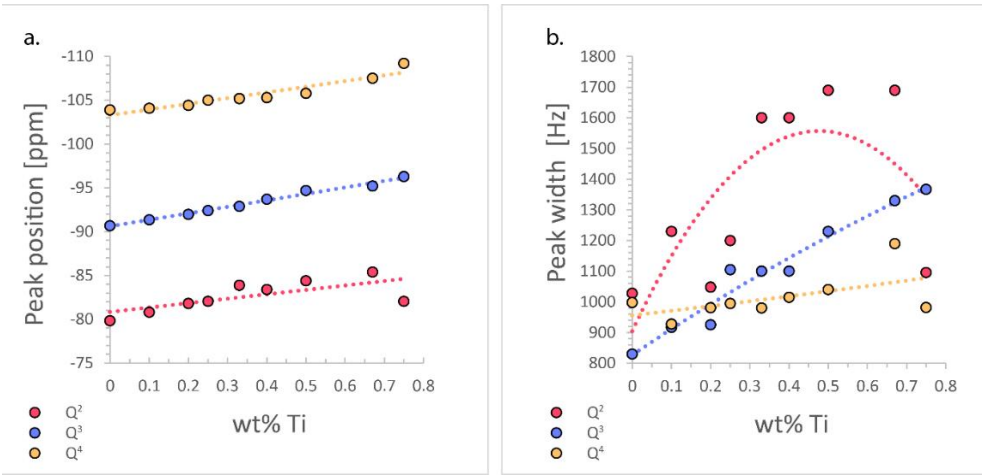

Figure 12. Peak position and peak width (a and b respectively) plotted against increasing Ti content in the sodium trisilicate glasses.

4.2. Glass network structure

The sodium trisilicate glass (NS_3) used in this study can be compared to other sodium-silicate glasses (figure 13). In the NS_4 and NS_8 glasses (Ackerson et al. 2020), the peaks of the Q^4 species are already more profound. This can clearly be seen in figure 13c where the Q^4 peak clearly increases with higher Si content. Despite the NMR data from (Ackerson and Mysen 2020) are informative about the change in Q species with increasing Ti content, the added Ti replaced both Na (NM) and Si (NF). This might compremise the direct effect from Ti to the glass structure. As was observed in the results

section figure 3, this effect is visible. However, a small variation in Si content does not change the shape of the spectrum too much.

In the obtained NMR data, it seems that the network polymerization increases with increasing Ti content as the Q^4 peak represents the amount of 4-coordinated $^{[4]}Si$. In (Lesher 2010) the activation energy for diffusivity is plotted with the degree of polymerization. From this paper it can be concluded that less activation energy is required for diffusion when Na is present in a more polymerized melt. When it comes to adding Ti in sodium-silicate melts the polymerization increases as can be observed in the ^{29}Si and ^{17}O NMR results. Therefore, increasing the Ti content in the melt could decrease the activation energy that is required for diffusion making it easier for Na to diffuse in a more polymerized melt. Besides a decrease in activation energy for Alkali elements like Na, for network formers (Si, O) in the melt, the activation energy increases. Hence, the opposite from Na can be assumed for the diffusion of Ti. The trend for transition metals (Ti, Co, Fe, Mn) is similar to that of the network formers thus for Ti as a NF and a transition metal, diffusion could become more difficult when more is added to the melt. As lunar glass can contain high concentrations of Ti, it could be interesting to know if Ti acts as a NF($^{[4]}Ti$, $^{[5]}Ti$) or a NM($^{[5]}Ti$, $^{[6]}Ti$), under lunar mantle pressure and temperature conditions. As high pressure studies have been performed in(Lee 2004), where the aluminium and silicon coordination both

increase with increasing pressure, this could definitely be the case for titanium as well.

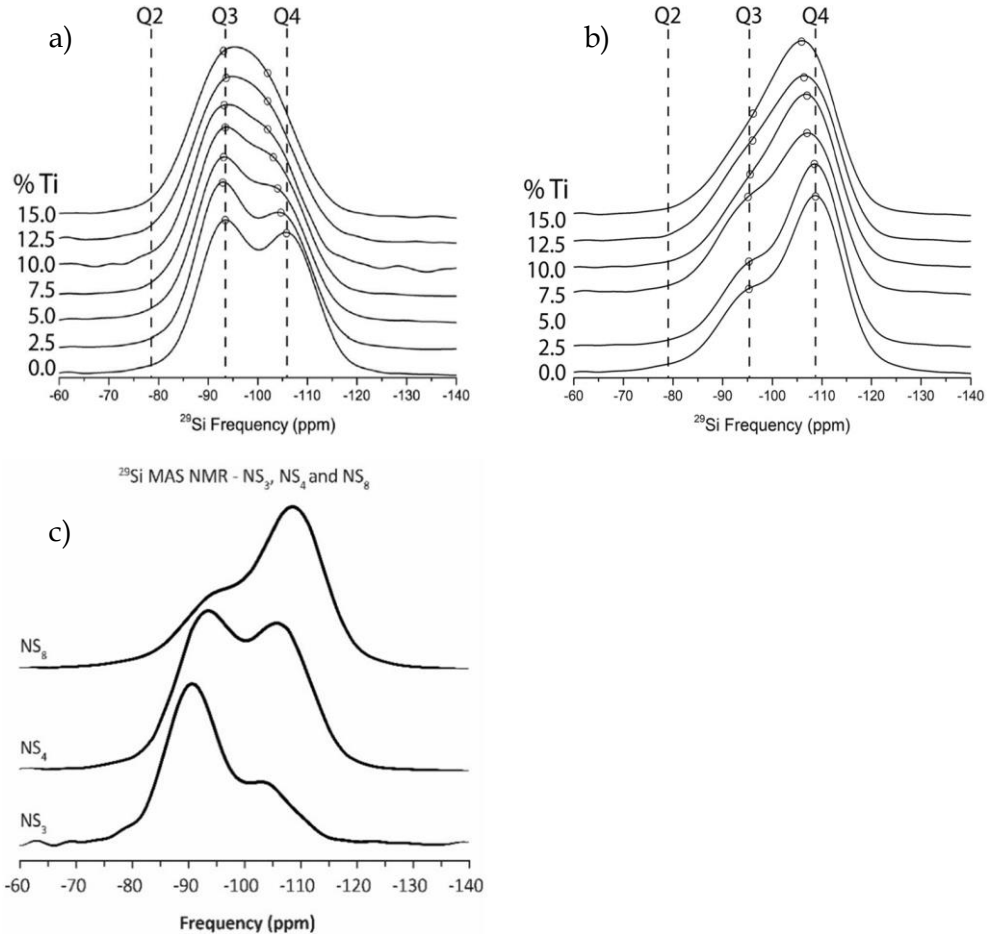

Figure 13. ^{29}Si MAS NMR spectra for NS_4 (a) and NS_8 (b) glass with increasing Ti content up to 15.0 mol% Ti (Ackerson et al. 2020). In figure c the NS_3 sample from this study is compared to both NS_4 and NS_8 from figures a and b.

4.3. Geological implications

As it is believed that the ilmenite-bearing cumulates(IBC) triggered the Rayleigh-Taylor instability in the lunar mantle, the high density of this material would cause a large scale lunar mantle overturn (Zhao et al. 2019). In order to understand how the titanium rich layer would interact with other melts deeper inside the mantle is very important to better understand the early magnetic field of the Moon, the origin of the chemistry of lunar mare basalts that are being observed on the lunar surface and if there is a partial melt layer at the core-mantle boundary.

Titanium incorporation in melts should increase the network polymerization, as the evidence for this is shown in the NMR spectroscopy data in this study. With this, the viscosity of the melt that corresponds to the glass is expected to increase with increasing Ti content. A study by (Liška et al. 1996) shows that there is indeed a positive correlation between the viscosity and the Ti content in Ti-bearing sodium trisilicate glass with the composition $(25 - x)Na_2O : xTiO_2 : 75SiO_2$ glasses (X = 0, 1, 2.5, 5, 7.5 and 10). Also, the configurational entropy[$S_{conf}(T_g)$] and free hindrance energy(B_e) give an indication that there is a change in the structural role Ti plays in these glasses. They concluded that the sudden change in configurational entropy and free hindrance energy can be caused by a coordination change from $^{[6]}$Ti to $^{[4]}$Ti, based on a previous study by (Mysen and Neuville 1995).

The presence of alkali metals(e.g., Na, Ca, K) is very important for the partitioning of Ti into rock-forming silicates and oxides. [4]Ti in rhyolitic melts can easily enter the tetrahedral sites of alkali-rich amphiboles. On the other hand, [6]Ti in basaltic melts finds its way into the octahedral sites in alkaline-earth-rich pyroxenes (Farges and Brown 1997).

A higher viscosity results in a lower Rayleigh number as they are inversely proportional to one another.

$$Ra_{\text{ref}} = \frac{\alpha \rho g \Delta T D^3}{\kappa \eta_{\text{ref}}}$$

This leads to the expectations that the lunar mantle has a smaller degree of mixing than other planetary bodies like Earth. This could have led to a less mixed mantle ocean before full solidification (Maurice et al. 2017). Less upper mantle mixing could also affect the previously believed timespan of magma ocean cooling to be much longer as heat is meanly being transferred with conduction.

Considering Ti coordination for shallow depth with lower pressure range is [4]Ti and [5]Ti, less mantle mixing is expected while the IBC layer descends into the lunar mantle. However, it can be expected that with increasing depth and thus pressure, the coordination of Ti changes to [6]Ti. As a result of this, mixing between the IBC layer and ambient mantle material could increase with depth as [6]Ti is a network modifier.

From the study by (Vander Kaaden et al. 2015), the lunar green glass containing low concentrations of Ti has a higher density then the lunar black glass with higher concentrations of Ti at greater pressure conditions. This could be the reason why low Ti concentrated melt resulted from increased mixing of the IBC layer at greater depth, can remain at the lower mantle. This idea of increased mixing with greater depth can be supported by geophysical models of IBC melting (Zhao et al. 2019). This study shows that the partial melting of the ICB layer with a density of 3719 kgm^{-3}, as a result of melting by radioactive decay in the KREEP layer, descends into the mantle and starts mixing once it reaches greater depths. In these models a partial melt layer at the lower mantle occurs.

From this study and in accordance with previous suggestions from other studies, it is predicted that less mixing of the lunar mantle ocean occurred where high Ti concentrations are present because of their effect of increasing the network polymerization of melts with increasing Ti content. As the results in this study are based on simplified compositions and performed at 1 atm pressure conditions, further research related to NMR spectroscopy for more complex and high-pressure samples would yield even more promising results.

5. Conclusion

5.1. The effect of Ti on sodium tri- and aluminosilicate glasses.

The observed structural details in this study represent the 1 atm pressure conditions. From the ^{29}Si NMR experiments, high Ti concentration show in a peak intensity increase that represents the Q^4 species fractionation. This becomes the dominant fraction, indicating a significant change in the network polymerization of the glass. This implies that the network polymerization is highly dependent on the Ti content as this element seems to act as a network former. Very important information from the ^{17}O NMR data is that the Ti and Al nuclei avoid being each other's next nearest neighbour within the silicate glass network. This confirms previous studied related to the titanium-aluminium avoidance. Also, a significant portion of the glass consists of Ti-O-Si bonds confirming the ^{29}Si NMR data that titanium is a network former. The ^{27}Al NMR data does provide knowledge about the increased ordering of the melt with increasing Ti content. This is due to the observation that peak width narrowing was observed for both MAS and isotropic dimensions.

5.2. Lunar mantle dynamics implications

Titanium incorporation in melts increases the network polymerization as it is mostly $^{[4]}Ti$, and therefore implies a higher viscosity of the Ti rich upper mantle. Because of the Lunar mantle overturn model driven by the higher

density of the IBC layer, the temperature and pressure on these melts increase with depth causing a Ti coordination change from $^{[4]}$Ti to $^{[6]}$Ti. The Ti becomes a network modifier and therefore lowers the viscosity of the melt with increased mantle mixing as a result. The now mixed lower mantle has a lower Ti concentration compared to the original IBC layer and therefore has a higher density as the low Ti melts are thought to be more compressible. This could be the reason why there is a dense partial melt layer at the core-mantle boundary of the Moon.

6. Appendix section

Appendix A. Lunar glass compositions

	SiO_2	TiO_2	Al_2O_3	Cr_2O_3	FeO	MnO	MgO	CaO	Na2O	K2O	Mg#
Apollo15 Green glass[a]	48.00	**0.26**	7.74	0.57	16.50	0.19	18.20	8.57	n.d.	n.d.	66.30
Apollo14 Yellow glass[a]	40.80	**4.58**	6.16	0.41	24.70	0.30	14.80	7.74	0.42	0.10	51.60
Apollo17 Orange glass[a]	38.50	**9.12**	5.79	0.69	22.90	n.a.	14.90	7.40	0.38	n.d.	53.70
Apollo15 Red glass[b]	35.60	**13.80**	7.15	0.77	21.90	0.25	12.10	7.89	0.49	0.12	49.60
Apollo14 Black glass[a]	34.00	**16.40**	4.60	0.92	24.50	0.31	13.30	6.90	0.23	0.16	49.20

n.a. not analyzed; n.d. not detected
[a](Delano 1986b)
[b](Krawczynski and Grove 2012)

Appendix B. Schematic figure of the internal structure of the Moon (Wieczorek 2006).

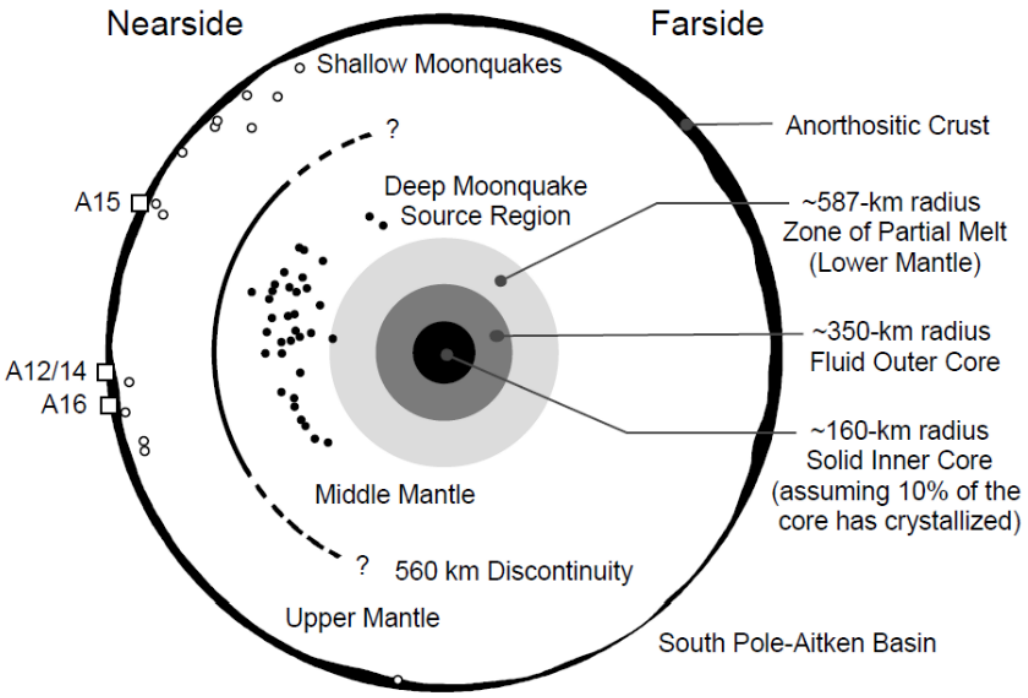

Appendix C. P and S wave velocity models of the lunar mantle. The model is based on the non-linear Bayesian inversion of (Khan et al. 2014).

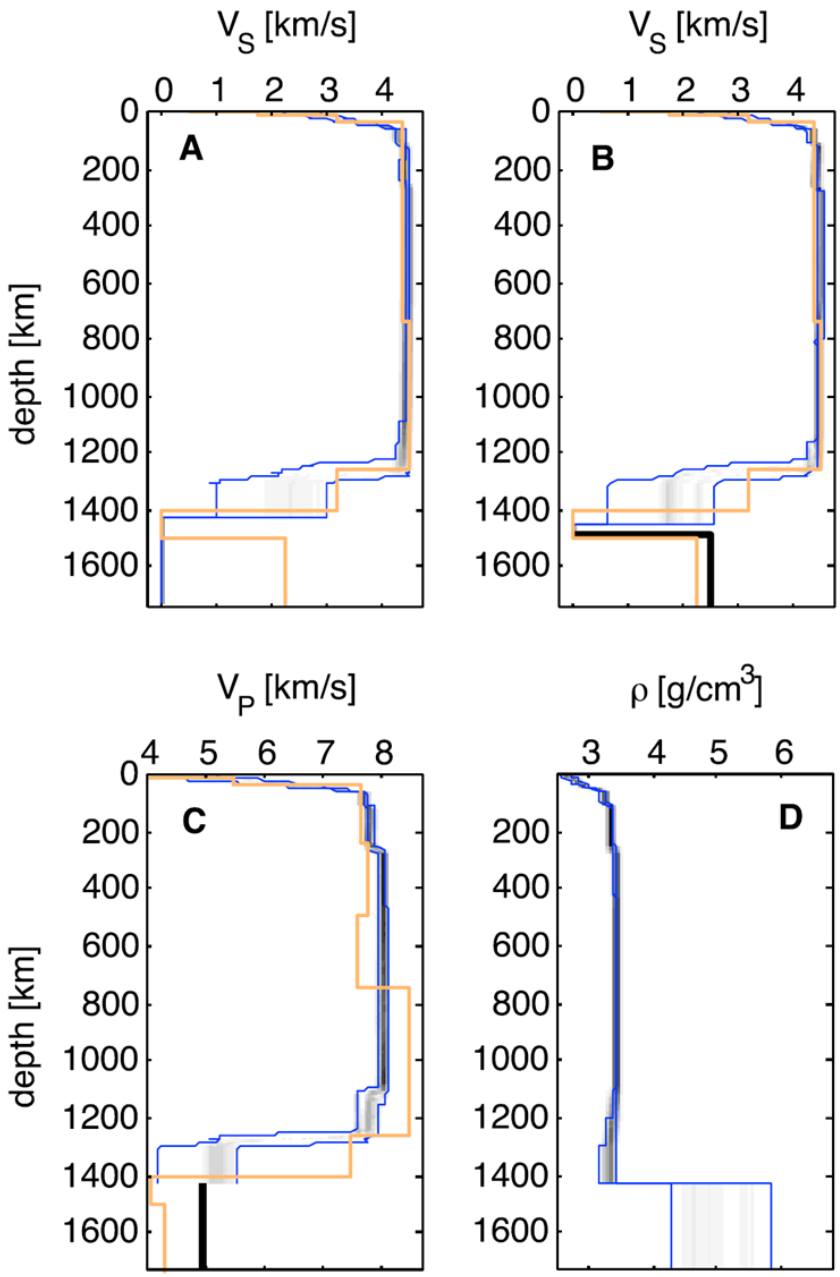

Appendix D. Thermal structure of the lunar interior (Khan et al. 2014).

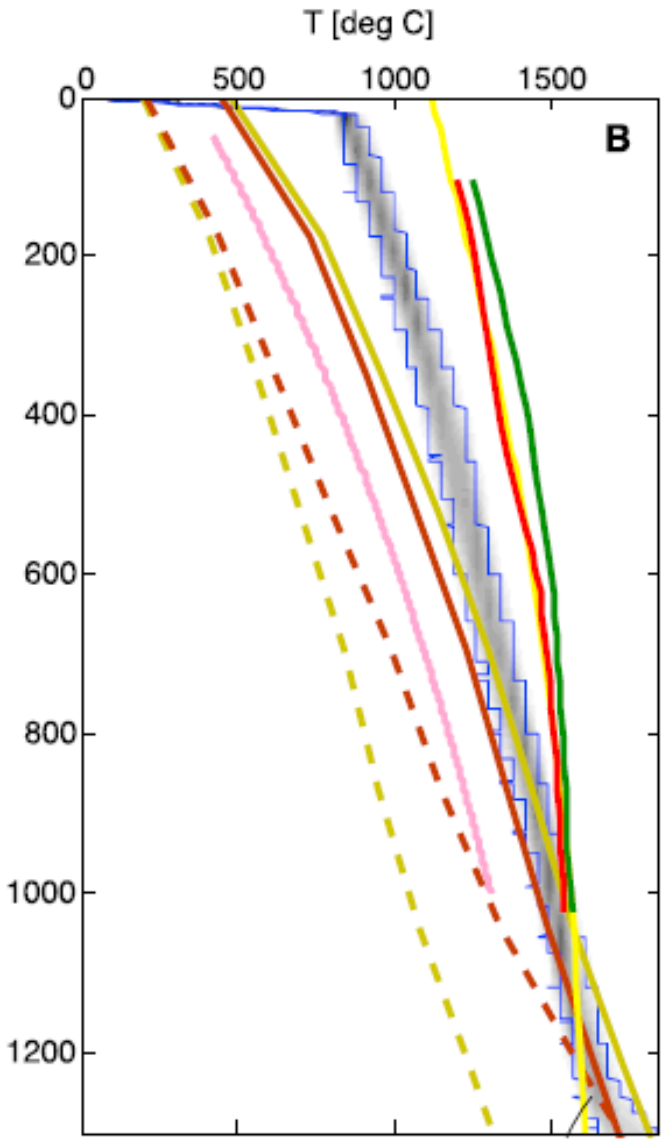

Appendix E. Phase diagram of SiO2 TiO2 and Na2O. The SiO2 concentration is fixed at 75% while TiO2 increases and Na2O decreases. Modified from: (Ackerson et al. 2020) and (Glasser and Marr 1979).

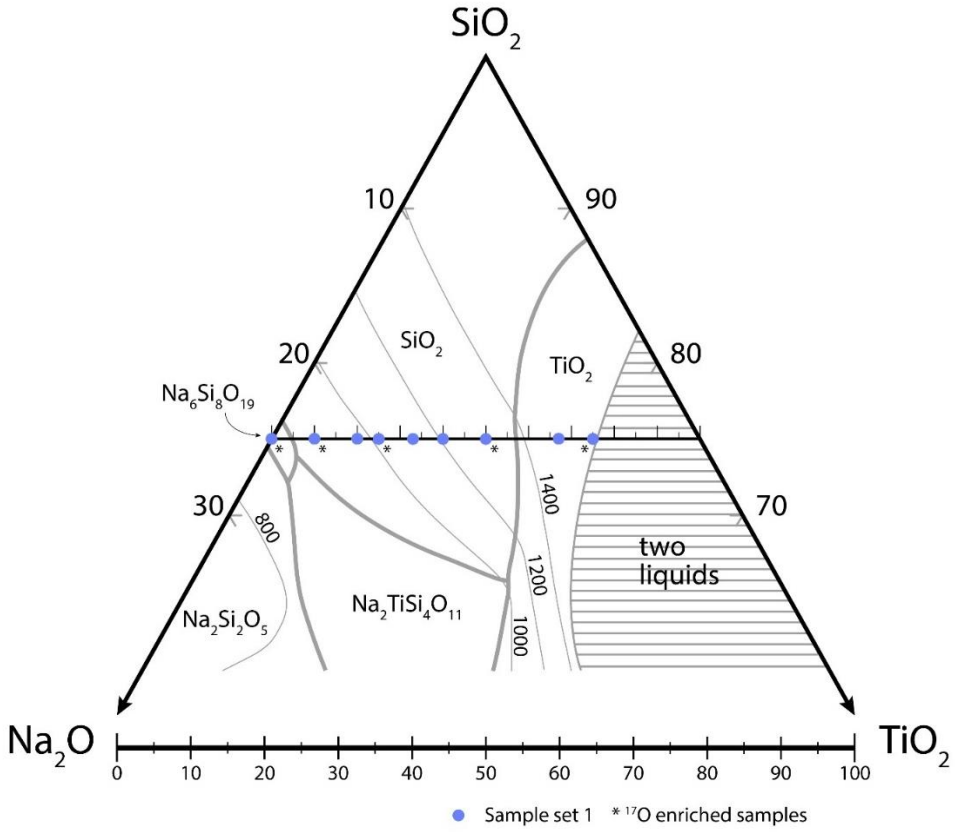

Appendix F. Attended classes

2020

Advanced Mineralogy and Lab.: Special Topics and Experiments in Mineralogy
Seminar in Earth and Environmental Sciences Topics

2021

Advanced Mineralogy and Lab.: Mineral Physics
Stable Isotope Geochemistry and Lab.
Geophysics

2022

Advanced Mineralogy and Lab.: Quantum Chemical Calculations

Appendix G. Conference List

Domestic Conferences

El Ghazaoui, E. Lee, J. and Lee, S. K., Effect of Ti on the network polymerization in Ti-bearing sodium silicate glass using 29Si NMR spectroscopy.

Annual Joint Conference of Petrological Society of Korea and Mineralogical Society of Korea, Virtual meeting, August 26, 2021. (Poster presentation).

References

Ackerson, M. R., G. D. Cody & B. O. Mysen (2020) Si-29 solid state NMR and Ti K-edge XAFS pre-edge spectroscopy reveal complex behavior of Ti in silicate melts. *Progress in Earth and Planetary Science,* 7.

Ackerson, M. R. & B. O. Mysen (2020) Experimental observations of TiO2 activity in rutile-undersaturated melts. *American Mineralogist,* 105**,** 1547-1555.

Delano, J. 1979. Apollo 15 green glass-chemistry and possible origin. In *Lunar and Planetary Science Conference Proceedings*, 275-300.

Delano, J. W. 1986. Abundances of cobalt, nickel, and volatiles in the silicate portion of the Moon. In *Origin of the Moon*, 231-247.

Elkins-Tanton, L. T., N. Chatterjee & T. L. Grove (2003) Experimental and petrological constraints on lunar differentiation from the Apollo 15 green picritic glasses. *Meteoritics & Planetary Science,* 38**,** 515-527.

Farges, F. & G. E. Brown (1997) Coordination chemistry of titanium(IV) in silicate glasses and melts .4. XANES studies of synthetic and natural volcanic glasses and tektites at ambient temperature and pressure. *Geochimica Et Cosmochimica Acta,* 61**,** 1863-1870.

Farges, F., G. E. Brown, A. Navrotsky, H. Gan & J. J. Rehr (1996a) Coordination chemistry of Ti(IV) in silicate glasses and melts .2. Glasses at ambient temperature and pressure. *Geochimica Et Cosmochimica Acta,* 60**,** 3039-3053.

Farges, F., G. E. Brown, A. Navrotsky, H. Gan & J. R. Rehr (1996b) Coordination chemistry of Ti(IV) in silicate glasses and melts .3. Glasses and melts from ambient to high temperatures. *Geochimica Et Cosmochimica Acta,* 60**,** 3055-3065.

Farges, F., G. E. Brown & J. J. Rehr (1996c) Coordination chemistry of Ti(IV) in silicate glasses and melts .1. XAFS study of titanium coordination in oxide model compounds. *Geochimica Et Cosmochimica Acta,* 60**,** 3023-3038.

Farges (1997) Ti K-edge XANES studies of Ti coordination and disorder in oxide compounds: Comparison between theory and experiment. *Physical Review B,* 56**,** 1809-1819.

Fogel, R. A. & M. J. Rutherford (1995) Magmatic volatiles in primitive lunar glasses: I. FTIR and EPMA analyses of Apollo 15 green and yellow

glasses and revision of the volatile-assisted fire-fountain theory. *Geochimica et Cosmochimica Acta,* 59**,** 201-215.

Goins, N. R., A. Dainty & M. Toksöz (1981) Lunar seismology: The internal structure of the Moon. *Journal of Geophysical Research: Solid Earth,* 86**,** 5061-5074.

Grillo, M. E. & J. Carrazza (1997) Computer Simulation Study of Aluminum Incorporation in the Microporous Titanosilicate ETS-10. *The Journal of Physical Chemistry B,* 101**,** 6749-6752.

Heiken, G. (1975) Petrology of lunar soils. *Reviews of Geophysics,* 13**,** 567-587.

Hirschmann, M. M. (2000) Mantle solidus: Experimental constraints and the effects of peridotite composition. *Geochemistry, Geophysics, Geosystems,* 1**,** n/a-n/a.

Khan, A., J. A. Connolly, A. Pommier & J. Noir (2014) Geophysical evidence for melt in the deep lunar interior and implications for lunar evolution. *Journal of Geophysical Research: Planets,* 119**,** 2197-2221.

Khan, A., J. A. D. Connolly, J. Maclennan & K. Mosegaard (2007) Joint inversion of seismic and gravity data for lunar composition and thermal state. *Geophysical Journal International,* 168**,** 243-258.

Kiani, A., L. S. Cahill, E. A. Abou Neel, J. V. Hanna, M. E. Smith & J. C. Knowles (2010) Physical properties and MAS-NMR studies of titanium phosphate-based glasses. 120**,** 68-74.

Kuskov, O. & V. Kronrod (1998) Constitution of the Moon: 5. Constraints on composition, density, temperature, and radius of a core. *Physics of the Earth and Planetary Interiors,* 107**,** 285-306.

Kuskov, O. L., V. A. Kronrod & L. L. Hood (2002) Geochemical constraints on the seismic properties of the lunar mantle. *Physics of the Earth and Planetary Interiors,* 134**,** 175-189.

Lee, D.-C., A. N. Halliday, I. Leya, R. Wieler & U. Wiechert (2002) Cosmogenic tungsten and the origin and earliest differentiation of the Moon. *Earth and Planetary Science Letters,* 198**,** 267-274.

Lee, S. K. (2004) Structure of Silicate Glasses and Melts at High Pressure: Quantum Chemical Calculations and Solid-State NMR. *The Journal of Physical Chemistry B,* 108**,** 5889-5900.

Lesher, C. E. (2010) Self-diffusion in Silicate Melts: Theory, Observations and Applications to Magmatic Systems. *Reviews in Mineralogy and Geochemistry,* 72**,** 269-309.

Liška, M., P. Šimurka, J. Antalík & P. Perichta (1996) Viscosity of titania-bearing sodium silicate melts. *Chemical Geology,* 128**,** 199-206.

Lognonné, P., J. Gagnepain-Beyneix & H. Chenet (2003) A new seismic model of the Moon: implications for structure, thermal evolution and formation of the Moon. *Earth and Planetary Science Letters,* 211**,** 27-44.

Longhi, J. (2006) Petrogenesis of picritic mare magmas: constraints on the extent of early lunar differentiation. *Geochimica et Cosmochimica Acta,* 70**,** 5919-5934.

Maekawa, H., T. Maekawa, K. Kawamura & T. Yokokawa (1991) The structural groups of alkali silicate glasses determined from 29Si MAS-NMR. *Journal of Non-Crystalline Solids,* 127**,** 53-64.

Maurice, M., N. Tosi, H. Samuel, A.-C. Plesa, C. Hüttig & D. Breuer (2017) Onset of solid-state mantle convection and mixing during magma ocean solidification. *Journal of Geophysical Research: Planets,* 122**,** 577-598.

Maurice, M., N. Tosi, S. Schwinger, D. Breuer & T. Kleine (2020) A long-lived magma ocean on a young Moon. *Science Advances,* 6**,** eaba8949.

Morard, G., J. Bouchet, A. Rivoldini, D. Antonangeli, M. Roberge, E. Boulard, A. Denoeud & M. Mezouar (2018) Liquid properties in the Fe-FeS system under moderate pressure: Tool box to model small planetary cores. *American Mineralogist,* 103**,** 1770-1779.

Mysen, B. & D. Neuville (1995) Effect of temperature and TiO2 content on the structure of Na2Si2O5□Na2Ti2O5 melts and glasses. *Geochimica et Cosmochimica Acta,* 59**,** 325-342.

Nakamura, Y., G. V. Latham & H. J. Dorman (1982) Apollo lunar seismic experiment—Final summary. *Journal of Geophysical Research: Solid Earth,* 87**,** A117-A123.

Nienhuis, E. T., J. Marcial, T. Robine, C. Le Losq, D. R. Neuville, M. C. Stennett, N. C. Hyatt & J. S. McCloy (2020) Effect of Ti4+ on the structure of nepheline (NaAlSiO4) glass. *Geochimica Et Cosmochimica Acta,* 290**,** 333-351.

Rai, N., J.-P. Perrillat, M. Mezouar, A. Colin, S. Petitgirard & W. van Westrenen (2019) In situ Viscometry of Primitive Lunar Magmas at High Pressure and High Temperature. *Frontiers in Earth Science,* 7.

Reid, J. E., A. Suzuki, K.-I. Funakoshi, H. Terasaki, B. T. Poe, D. C. Rubie & E. Ohtani (2003) The viscosity of CaMgSi2O6 liquid at pressures up to 13GPa. *Physics of the Earth and Planetary Interiors,* 139**,** 45-54.

Ridley, W. I., A. M. Reid, J. L. Warner & R. W. Brown (1973) Apollo 15 green glasses. *Physics of the Earth and Planetary Interiors,* 7**,** 133-136.

Righter, K. & C. Shearer (2003) Magmatic fractionation of Hf and W: constraints on the timing of core formation and differentiation in the Moon and Mars. *Geochimica et Cosmochimica Acta,* 67**,** 2497-2507.

Sato, M. 1979. The driving mechanism of lunar pyroclastic eruptions inferred from the oxygen fugacity behavior of Apollo 17 orange glass. In *Lunar and Planetary Science Conference Proceedings*, 311-325.

Shearer, C. K., P. C. Hess, M. A. Wieczorek, M. E. Pritchard, E. M. Parmentier, L. E. Borg, J. Longhi, L. T. Elkins-Tanton, C. R. Neal & I. Antonenko (2006) Thermal and magmatic evolution of the Moon. *Reviews in Mineralogy and Geochemistry,* 60**,** 365-518.

Solomon, S. C. & J. Longhi. 1977. Magma oceanography. I-Thermal evolution. In *Lunar and planetary science conference proceedings*, 583-599.

Taylor, S. R. 1982. *Planetary science: A lunar perspective*. Lunar and Planetary Institute Houston.

Vander Kaaden, K. E., C. B. Agee & F. M. McCubbin (2015) Density and compressibility of the molten lunar picritic glasses: Implications for the roles of Ti and Fe in the structures of silicate melts. *Geochimica et Cosmochimica Acta,* 149**,** 1-20.

Wagner, T. P. & T. L. Grove (1997) Experimental constraints on the origin of lunar high-Ti ultramafic glasses. *Geochimica et Cosmochimica Acta,* 61**,** 1315-1327.

Wang, Y., T. Sakamaki, L. B. Skinner, Z. Jing, T. Yu, Y. Kono, C. Park, G. Shen, M. L. Rivers & S. R. Sutton (2014) Atomistic insight into viscosity and density of silicate melts under pressure. *Nature Communications,* 5.

Warren, P. H. (1985) The magma ocean concept and lunar evolution. *Annual Review of Earth and Planetary Sciences,* 13**,** 201-240.

Weber, R. C., P.-Y. Lin, E. J. Garnero, Q. Williams & P. Lognonné (2011) Seismic Detection of the Lunar Core. *Science,* 331**,** 309-312.

Wieczorek, M. A. (2006) The Constitution and Structure of the Lunar Interior. *Reviews in Mineralogy and Geochemistry,* 60**,** 221-364.

Yarker, C. A., P. A. V. Johnson, A. C. Wright, J. Wong, R. B. Greegor, F. W. Lytle & R. N. Sinclair (1986) Neutron diffraction and exafs evidence for TiO5 units in vitreous K2O ·TiO2 ·2SiO2. 79**,** 117-136.

Zhao, Y., J. De Vries, A. P. Van Den Berg, M. H. G. Jacobs & W. Van Westrenen (2019) The participation of ilmenite-bearing cumulates in lunar mantle overturn. *Earth and Planetary Science Letters,* 511**,** 1-11.